University of Nevada, Reno

Identifying Indicators and Timescales of Agricultural Drought in the Northeast United States using Crop Area-weighted Drought Indices

A thesis submitted in partial fulfillment of the

requirements for the degree of Master of Science in

Atmospheric Science

by

Shuang Xia

Dr. Daniel McEvoy/Thesis Advisor

May, 2022

THE GRADUATE SCHOOL

We recommend that the thesis
prepared under our supervision by

SHUANG XIA

entitled

Identifying Indicators and Timescales of Agricultural Drought in the Northeast United States using Crop Area-weighted Drought Indices

be accepted in partial fulfillment of the
requirements for the degree of

MASTER OF SCIENCE

Daniel McEvoy, Ph.D.
Advisor

Mike Hobbins, Ph.D.
Committee Member

Justin Huntington, Ph.D.
Graduate School Representative

David W. Zeh, Ph.D., Dean
Graduate School

May, 2022

Abstract

Critical indices of agricultural drought in the Northeast United States (Northeast) are examined with a particular focus on the drought events in 2016 and 2020. We evaluate relationships of drought indices that are based on precipitation (PRCP), soil moisture (SM), and evaporative demand (E_0) and their optimal timescales to agricultural-impacts data. We resampled forty years (1981-2020) of these daily climate drivers onto crop-cover maps provided by the National Agricultural Statistics Service (NASS) and computed standardized drought indices, namely the Standardized Precipitation Index (SPI), the Standardized Soil Moisture Index (SSMI), and the Evaporative Demand Drought Index (EDDI). Further indices that reflect actual evapotranspiration (ET) and the balance between PRCP and E_0 — the Landscape Evaporative Response Index (LERI) and the Standardized Precipitation-Evapotranspiration Index (SPEI), respectively--were also included. Indices were estimated at timescales ranging from one week to twelve months. All climate drivers were averaged to state and county levels before their use in estimating the drought indices. Five of the most widely cultivated crops in the Northeast were selected--the most prominent being hay and pasture. Forty years (1981-2020) of annual hay yield and twenty-six years (1995-2020) of weekly pasture-condition records were retrieved from NASS. Hay yields were detrended and correlated to each set of drought indices, while pasture conditions were compared to the progression of indices within the drought years of 2016 and 2020. Results show the strongest correlation (R_{max}) around 0.5-0.7 between drought indices and hay yield, with SPI correlations being positive and

EDDI correlations negative. The R_{max} values and associated distribution of dates and timescales were derived for states and counties and exhibited distinct regional spatial variation. Hay yield showed the strongest response to shorter timescales for SSMI and EDDI than for SPI and SPEI. Weekly pasture conditions in most states exhibited a strong response to the 2016 and 2020 droughts. Characteristics of how the degradation of pasture through the growing season tracks the progression of drought indices across different states were examined. Respectively, pasture conditions show the strongest response to 1- to 2-week SSMI, 2-week to 1-month EDDI, and 1- to 3-month SPI. At the 1-week timescale, fluctuations of LERI generally tracked fluctuations of SSMI throughout both 2016 and 2020. The times when major pastureland degradations began were usually accompanied by abnormally low LERI, low SSMI, and high EDDI, regardless of SPI.

Table of Contents

List of Tables

List of Figures

1. Introduction

1.1. Background

1.1.1. Recent Drought and Impact in the United States (US)

Drought is among the most disastrous and costly weather-related hazards with its far-reaching effects. Compared to other extreme hydrologic events, such as floods, drought is characterized by slower development, longer duration, wider area, and a broader scope of the people affected. However, the causal mechanisms and contributing factors of drought can operate at a wide range of temporal and spatial scales (Kiem et al., 2016). Extreme drought events ranging from weeks to one year focused on the growing season are the primary target of this study. In this context, severe drought events have been reported across the continental US (CONUS) in recent decades, including the 2011 Texas drought, the 2012 central Great Plains drought, the 2011-15 California drought, the 2016 Southeastern US drought, and the 2016 and 2020 Northeastern US droughts (Hoerling et al., 2014; Lombard et al., 2020; Nielsen-Gammon, 2012; Park Williams et al., 2017; Seager et al., 2015; S. K. Sweet et al., 2017).

These events have caused huge losses with substantial impacts on various social and economic aspects, especially in the agricultural sector. For example, the initial loss estimates for the 2012 Great Plains drought were $12 billion (Henderson & Kauffman,

2012). According to the US Department of Agriculture (USDA), the final US 2012 corn production was 33% below USDA's expectation at the growing season's start (USDA, 2013). Severe droughts over North America have also led to massive water shortages: the storage level of lakes monitored by the Lower Colorado River Authority hit a record low during the 2011-12 Texas drought due to inflows at only 10% of average (Grigg, 2014); record-low snowpack and storage levels were also found across California for the 2014 statewide drought (AghaKouchak et al., 2014). Some drought events may contribute to an increased wildfire frequency: the 2011 Southwest drought led to a record burnt area in Arizona and New Mexico (Williams et al., 2014); and wildfires that emerged in Tennessee during the 2016 Southeastern drought cost 2,400 structures and 14 lives, making it the deadliest wildfire event in the Eastern US since 1947 (Praskievicz & Sigdel, 2021). In addition, droughts are often accompanied by unemployment: due to the 2011-2015 California drought, ~17,100 people from which ~7,500 directly in agriculture lost their jobs in 2014; the numbers in 2015 during this drought were respectively ~21,000 and ~10,100 (Howitt et al., 2015).

Under the background of global warming, not only is the frequency of drought events increasing (Sheffield & Wood, 2008), but their characteristics are changing at both global and regional scales (Huang et al., 2016; Trenberth et al., 2014). In the coming decades, there will be urgent needs in improving drought early warning and mitigation efforts. Many efforts have already been implemented to meet diverse types of demands from decision-makers. Two successful examples are the Drought Early Warning Systems (DEWS) of NOAA's National Integrated Drought Information System (NIDIS, 2020)

and the drought-monitoring tools maintained by the National Drought Mitigation Center (NDMC, 2021). Drought monitoring plays a crucial role in understanding the mechanism and regional manifestation of drought, as well as mitigating its impacts. Such knowledge may also aid in predicting the severity of potential damage caused by an upcoming drought. Additionally, the existing records of historical dry events can also be consolidated into archives to make statistical forecasts of the duration and frequency of drought (Sharma & Panu, 2012; Wetterhall et al., 2015).

1.1.2. Drought in The Northeastern US

The Northeast has more than 175,000 farms producing more than $21 billion worth of field crops annually (NRCC, 2017). By area, agricultural land cover in the Northeast breaks down as follows: 60% is forested; 11% is farmland; and 4% is pastureland (Bigelow & Borchers, 2017). By current practice, the state of New York (NY), Pennsylvania (PA), New Jersey (NJ), West Virginia (WV), Maryland (MD), Delaware (DE), and all the New England states comprise the Northeast Climate Region. However, current DEWS in the Northeast only covers New England and NY. This study expands the research area to include PA and NJ, considering their proximity and abundant agricultural resources (Figure 1).

Though infrequent, agricultural drought (as opposed to hydrologic drought; discussed in section 1.1.3) in the Northeast may possess distinct characteristics than in other parts of the US. The region is generally wetter and cooler than other major agricultural production areas in the country (e.g., Midwest, California; (Dupigny-Giroux

et al., 2018)). Due to most agriculture being rainfed rather than irrigated, climate and variations of weather are critical for farmland SM and the forming of agricultural drought in the Northeast (Dieter, 2018). One example is the drought during the 2016 growing season (see also Section 3.2.1). In NY, scarce snow from December 2015 through February 2016 was accompanied by severe dry conditions during the summer of 2016, causing major damage to rainfed crops and pasture acreages (S. K. Sweet et al., 2017). Such a trend underscored the urgent need for early warning information and drought mitigation in the region.

The worst drought in the Northeast recorded in the 20th century occurred between 1962 and 1966, affecting millions of people and creating a serious water-supply crisis (Barksdale, 1968). Although there is little evidence that the event is responsible for severe direct economic damage, it has since reshaped water management strategies in the Northeast (Degaetano, 1999). A deficit of PRCP was the primary factor contributing to this drought; however, temperatures at historical lows during the period prevented the situation from worsening (Namias, 1966). This drought was classified as a multi-year event mainly due to continuous negative annual values of the Palmer Drought Severity Index (PDSI). With the dynamic factors of the land-atmosphere interactions remaining uncertain, studies have attributed this event to both atmospheric circulation and sea surface temperature anomalies (Barlow et al., 2001; Seager, Pederson, et al., 2012).

Since the 1960s, the Northeast has experienced a long-term trend of increasing humidity (Seager, Pederson, et al., 2012). Ground observations and models have both indicated a moderate and steady PRCP increase in the area (Frumhoff et al., 2007). The

most recent multi-year dry period was the 1999-2004 drought that intermittently stretched across North America, also affecting the Northeast (Lotter et al., 2003; Seager, 2007). In general, global warming tends to intensify the hydrological circulation and make droughts and floods more frequent and severe (Seager, Naik, et al., 2012; Trenberth et al., 2014). Climate-model simulations suggest that such an increase in drought frequency and severity will be especially evident for the Northeast under continued warming (Giorgi et al., 2011; Hayhoe et al., 2007; Lickley & Solomon, 2018).

The mean temperature of summer 2016 in NY was 2.6 °F above the 20th century average, while the total precipitation was 0.46 inches below the 20th century average (NCDC, 2022). The anomalous weather had severe impacts on large agricultural areas in western NY and southern New England (Kaufman, 2016; Nosowitz, 2016; S. K. Sweet et al., 2017). A survey of over 200 farmers in NY suggests that, in 2016 alone, non-irrigated fields lost over 30% of yield, with some farmers reporting over 90% (S. Sweet & Wolfe, 2017). This drought occurred in three atypical ways. First, the drought period was established and extended quickly in early summer, despite average rains in May and July. Within the same year, the drought was alleviated by heavy winter rainfall and officially lifted in March 2017 based on the US Drought Monitor (USDM; (Moden, 2017)), making it more intense but much shorter in duration compared to those of the 1960s and 2000s. Second, a significant snowfall deficit in the previous winter and low snowmelt were factors contributing to groundwater depletion and low streamflow (S. K. Sweet et al., 2017). This depletion enhanced the establishment of drought at its early stage and accelerated its expansion. Finally, the drought was worse than PRCP data alone would

suggest (Orr, 2016). Record hot temperatures occurred during the growing season, which, in conjunction with the absence of rain, rapidly depleted SM to the crop-wilting threshold.

An increasing number of studies have found that drought in the Northeast is driven by multiple factors (e.g., snowpack, SM, land-atmosphere interactions) rather than PRCP deficits alone (Alessi et al., 2022; Frumhoff et al., 2008; Hayhoe et al., 2007; S. K. Sweet et al., 2017). With the rapid development and being focused on the growing season, features of the 2016 drought were reproduced by a similar drought event in 2020, except that the 2019-2020 winter snowfall was not as low as that in 2015-2016 (Lombard et al., 2020). Again, field crops were severely damaged with states in New England suffering the most (Erdman, 2020). Both the 2016 and 2020 droughts brought public attention to the phenomenon and its agricultural impacts.

Only a small fraction of crops is irrigated in the Northeast as irrigation in such a humid region is generally considered complementary – only used to secure more sensitive and specialty products like fruits and vegetables. The lack of irrigation systems highlights the need for drought information and early warning in the Northeast. Besides the USDM, the US government offers climate and agriculture services to meet various needs. Some examples are the monthly and seasonal drought outlooks provided by NOAA's Climate Prediction Center (CPC, 2021), the weekly streamflow and groundwater status map generated by the United States Geological Survey (USGS, 2021), and the real-time regional analyses maintained by the Northeast Regional Climate Center (NRCC, 2021). The integrated portals that collect and organize these data sources are

widely available to users. For example, the USDA maintains climate hubs for the Northeast region that features different drought maps, advice on mitigation practices, and occasional seminars (USDA, 2021).

In 2006, Congress approved NIDIS with inter-agency coordination and an integrated research mandate to establish regional DEWS. The Northeast DEWS (NE DEWS) was formed following the 2016 drought. It brought together more than 100 community leaders representing sectors ranging from water and agricultural management to local governments and watershed groups. The mission of the NE DEWS is to collaboratively improve drought early warning capacity and long-term drought resilience throughout New England and NY. Enhancing drought monitoring, forecasting, and research has been prioritized as the primary objective as necessary for the mission (NIDIS & NOAA, 2019).

Figure 1. Definition of the Northeast in this study (green). Deep green shows the NE DEWS region, while this study adds PA and NJ. (Map courtesy: NE DEWS – https://www.drought.gov/dews/northeast)

1.1.3. Drought Types

Droughts are generally classified into meteorological, hydrological, agricultural, socioeconomic, and ecological types (Crausbay et al., 2017; Mishra & Singh, 2010; Wilhite & Glantz, 1985).

Meteorological drought usually results from a PRCP deficit over a prolonged period, which originates from anomalies in large-scale atmospheric circulation patterns (Dai, 2011). Driving factors of such anomalies could be anomalous sea surface temperature (SST; (Giannini et al., 2003)), ocean-atmosphere interactions such as El Niño–Southern Oscillation (ENSO; (McCabe et al., 2008)), internal atmospheric variables such as semi-permanent pressure systems (Sousa et al., 2018), and other complex climate teleconnections. Other factors, such as land-atmosphere interactions or feedback, may also contribute to reduced PRCP and hence to meteorological drought (Fernando et al., 2016; Kam et al., 2014).

Agricultural drought is generally defined by a deficit in SM, which is crucial to plant water use during the growing season and strongly affects yield. Negative anomalies in SM are mainly caused by the preceding PRCP deficit or increased ET (Sheffield et al., 2004; Van Loon, 2015). Temperature, net incoming radiation, wind speed, and humidity can all cause variations in ET (Walter et al., 2001). Due to the lack of observation networks, SM data are generally estimated from hydrological models.

Hydrological drought is characterized by a decrease in streamflow, reservoir level, or groundwater level. Though the antecedent PRCP deficit plays a significant role

in forming such deficits, the existing local hydrological conditions, such as low water storage and snow accumulation are also important (Van Loon & Van Lanen, 2012).

Socioeconomic drought is associated with the supply and demand throughout economic activities (e.g., industrial materials, food security; (Wilhite & Glantz, 1985)), which preserves definitions of all above types while including the effect of human activities that may account for the drought (Wilhite, 2000).

Finally, ecological drought was defined as the water deficit that exceeds the vulnerability of ecosystems. Such vulnerability is driven by both humans and nature, while the impact of drought can be transferred between the two and generates feedback (Crausbay et al., 2017). It happens in sectors where human communities are closely connected to nature (e.g., air quality regulation, waste treatment, erosion prevention, recreation) (Millar & Stephenson, 2015).

Due to the multiple physical and socio-ecological interactions and imprecise definitions of drought (Collins et al., 2016), it is generally hard to quantify its impact. This study focuses on agricultural drought for several reasons. First, the main impact of agricultural droughts is damage to and loss of crop productivity. Response time of crops to drought varies widely, ranging from immediately at the drought onset to the lifetime of the drought, depending on the crop type, planting location, and cultivating strategies (Blum, 1996; Mounce et al., 2016; Simelton et al., 2009). Other signals like reduced streamflow or economic shock occur in the mature stage or the aftermath of drought events. Second, water availability as represented by SM plays an essential role in plant growth, especially during critical phenological phases (Bolten et al., 2009; Yang &

Zhang, 2006). SM is the central variable integrating the effects of the water supply (PRCP) and demand (ET) at a particular location, therefore a good criterion for estimating drought onset (Sun et al., 2015; Yuan et al., 2019). Finally, agricultural sectors are among the main users that benefit most from drought information (Ash et al., 2007; Trnka et al., 2020). Few studies to date have focused on using drought indices to depict agricultural droughts in the Northeast. A better understanding of drought conditions as they relate to agricultural productivity in the Northeast is one of the primary purposes of this study. In addition, it can add value to the NE DEWS.

1.2. Proposed Science Questions

The aims of this study are to connect crop yield and conditions to different climate drivers while identifying the key indicators and timescales of agricultural drought in the Northeast. Specifically, this paper attempts to reveal such connection and identification by addressing the following questions:

I. How does each drought index perform when compared to the yield of hay from a long-term record?

II. What are the most critical periods and timescales that relate each drought index to hay yield and drought-driven pastureland degradation?

III. How do drought indices evolve and interact during the recent drought years of 2016 and 2020?

1.3. Broader Impacts on the Scientific Community

The objective of this study is to gain a more comprehensive understanding of drought and its impacts on agriculture in the Northeast. This will be accomplished by determining the most relevant climate drivers and timescales of droughts in the region and examining the degradation of crop conditions during cases of agricultural drought. The outcomes will lead to a better understanding of drought monitoring, data management, and informed decision-making by local authorities and stakeholders. The

identification of appropriate timescales may potentially be used as a reference for water management services for the timing of drought mitigation. In addition, knowing the critical period of the year for drought impacts can help farmers better plan growth cycles, crop types, and management strategies. Funded by NIDIS and NE DEWS, this study is based on a NOAA Sector Application Research Program (SARP), which aims to identify the most effective indicators and the most suitable timescales for drought monitoring in the Northeast. The findings of this study have the potential to be incorporated into the next phase of the NE DEWS Strategic Plan and contribute to its priorities of enhancing drought monitoring and research and strengthening decision making for drought preparedness.

2. Data and Methods

2.1. Data

2.1.1. Physical Drivers and Indices as Drought Indicator

This study examines the physical drivers that affect crop water balance and agricultural drought (Dai et al., 2018; Narasimhan & Srinivasan, 2005; Sepulcre-Canto et al., 2012). Respectively, PRCP, SM, and E_0 represent the supply of, storage of, and demand for moisture at the surface and therefore represent the climate constraints on the surface water budget. Further, drought indices corresponding to these physical drivers can provide spatial and temporal assessments of the severity of dry anomalies (Hayes et al., 2011). Multi-scalar drought indices allow the user to select a timescale, or accumulation period, in order to examine droughts that extend across various periods, such as months or years. The most widely used indices that depend on either PRCP or E_0 alone are, respectively, the Standardized Precipitation Index (SPI; (McKee, 1995; McKee et al., 1993)) and the Evaporative Demand Drought Index (EDDI; (M. T. Hobbins et al., 2016; McEvoy et al., 2016)). Other widely used indices that involved the climate drivers that are the foci of this study are the Standardized Precipitation-Evapotranspiration Index (SPEI; (Vicente-Serrano et al., 2010)), which depends on the difference of PRCP - $E_{0;}$ the Empirical Standardized Soil Moisture Index (ESSMI, replaced by SSMI in section 2.2.1; (Carrão et al., 2016)) that depends solely on SM; and the Landscape Evaporative Response Index (LERI; (Rangwala et al., 2019)), which depends on ET. The

correspondence between climate drivers and the drought indices used in this study is illustrated in Figure 2. The methods for deriving these drought indices are detailed in section 2.2.1.

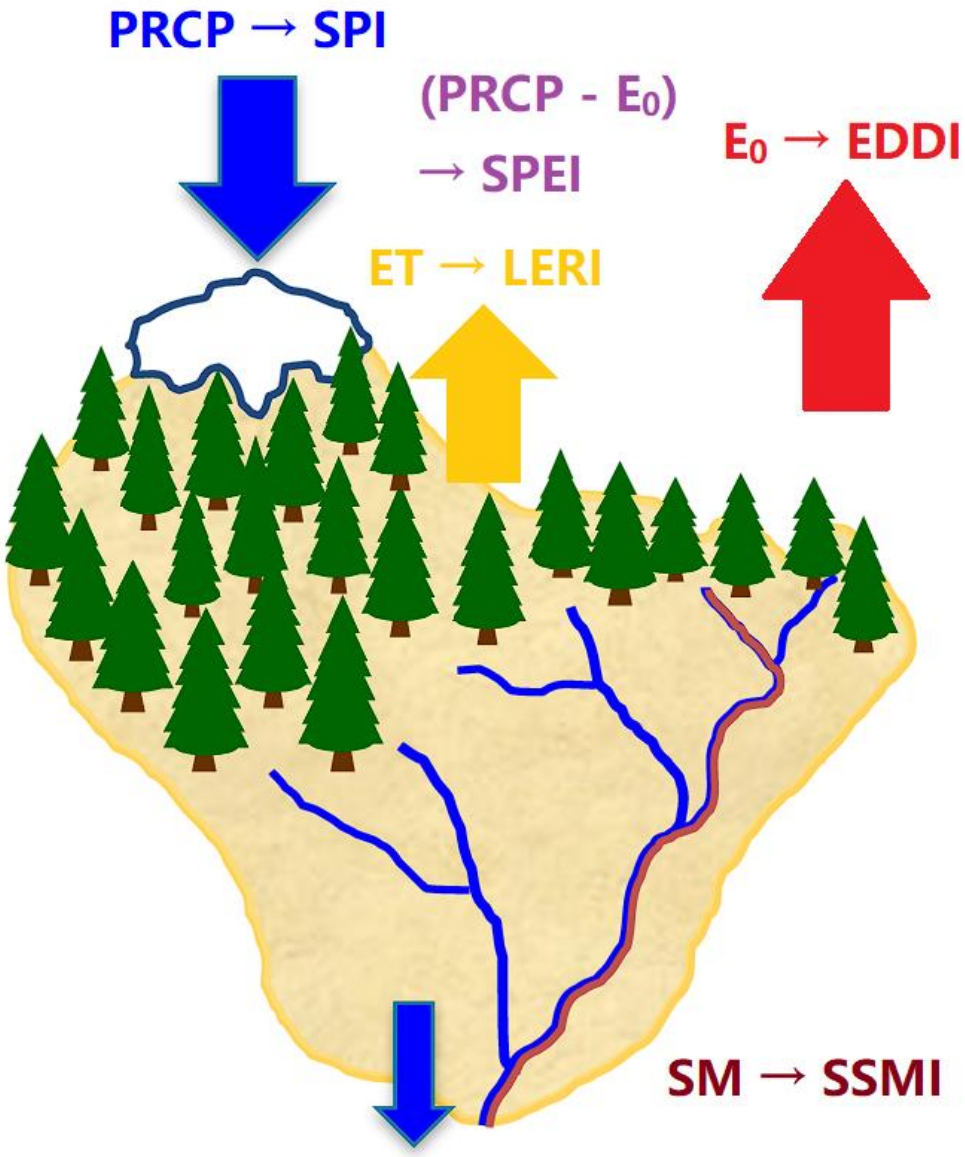

Figure 2. Conceptual representation of the physical drivers (PRCP, E_0, ET, and SM) of surface water balance and their correspondence to the drought indices (SPI, EDDI, SPEI, LERI, and SSMI) used in this study. (Adapted with permission from The EDDI User Guide – https://psl.noaa.gov/eddi/pdf/EDDI_UserGuide_v1.0.pdf)

Precipitation

The PRCP data used in this study were obtained from gridMET (Abatzoglou, 2013). The dataset has daily temporal frequency from 1980 to 2020, with a spatial resolution of ~4 km (1/24 degree) covering the CONUS. It combines spatial attributes of gridded climatic data from the Parameter-elevation Regressions on Independent Slopes Model (PRISM; (Daly et al., 1994)) with temporal attributes from the North American Land Data Assimilation System Phase 2 (NLDAS-2; (Xia et al., 2012)) using climate-facilitated interpolation. Only grid points inside the Northeast were selected in this study, with a buffer zone of two points around the edges of the study area retained for area weighting (weighting algorithm detailed in section 2.2.2).

Actual Evapotranspiration and the Landscape Evaporative Response Index

ET is defined as the sum of transpiration from vegetation and evaporation (and sublimation) from bare soil and water bodies. However, as a flux of water vapor from the land surface, ET is difficult to measure with a useful degree of accuracy and spatiotemporal resolution. The operational Simplified Surface Energy Balance (SSEBop) model developed by USGS compares land surface temperature from The Moderate Resolution Imaging Spectroradiometer (MODIS) against pre-defined dynamic boundary conditions to estimate the ET fraction (ET_f), which is the ratio of ET over the E_0 (Senay et al., 2013). The ET_f ratio is then multiplied by E_0 (detailed below) to generate ET. The

ET product provides an eight-day averaged map in the resolution of a 1 km grid for the period of 2000 to the present.

Compared to other drought indices derived in this study (section 2.2.1) that are based on PRCP, SM, and E_0, the index corresponding to ET is particularly limited by its period of record. This study directly uses LERI (https://psl.noaa.gov/leri/; (Rangwala et al., 2019)) as the measure of anomalies in ET. LERI uses ET derived from the SSEBop model (see section 2.1.1) that combines climatological E_0 with the ET_f generated by MODIS thermal imagery. Similar to its data source, LERI has temporal resolutions of monthly and eight days, with a period of record covering 2000 to the present, which is only around half of that for PRCP, SM, and E_0 (1980 to present). This study uses the eight-day LERI as it is almost in line with the frequency of weekly crop conditions record and the 1-week timescale of other indices.

Evaporative Demand and the Complementary Relationship

E_0 can be regarded as the upward demand for moisture at the interface of land and atmosphere. It is the potential flux, as it marks the maximal ET under ample moisture availability – figuratively, the "thirst of the atmosphere" (M. Hobbins et al., 2017). The effect of E_0 on drought is complex, depending on the type of drought and the regional moisture availability. Such complexity is particularly evident in humid regions like the Northeast. Generally, E_0 both drives and responds to ET depending on the moisture availability. A hypothesis known as the Complementary Relationship (CR) states the feedback mechanism between E_0 and ET (theoretical shape shown in Figure 3). When

there is sufficient SM, referred to as the energy-limited situation, E_0 and ET vary together as ET approaches E_0. If strong E_0 and ET continues with little incoming water compensation, SM will become insufficient to supply further ET. Under this moisture-limited situation, SM becomes the limiting factor of ET. The energy that would have been used for ET is now used to produce sensible heat flux, resulting in elevated E_0 diverging from the lacking ET (Bouchet, 1963; Huntington et al., 2011; Pendergrass et al., 2020). E_0 plays a crucial role in the CR hypothesis, and the amplifying feedback of E_0 from ET signifies the transition from an energy-limited situation to a moisture-limited situation. Therefore, it is necessary to consider E_0 as of equal importance as PRCP, SM, and ET regarding drought impact.

In practice, E_0 can be directly estimated using atmospheric-based metrics (e.g., atmospheric forcings on a prescribed reference crop surface (ET_0; (Allen et al., 1998)), or water evaporated from a metal pan modeled by meteorological data (E_{pan}; (Rotstayn et al., 2006)). The E_0 dataset used in this study is also downloaded from the gridMET dataset, in the same spatial and temporal resolutions as PRCP (~4 km, daily; see above). The formulation of E_0 used here applies a widely accepted algorithm using the ASCE Standardized Reference Evapotranspiration Equation (Walter et al., 2005):

$$E_0 \sim \frac{0.408\Delta(R_n - G) + \gamma \frac{C_n}{T + 273} u_2 (e_s - e_a)}{\Delta + \gamma(1 + C_d u_2)} \qquad (2-1)$$

In which C_n and C_d are reference constants for a 0.5-m tall crop like full-cover alfalfa. Based on the Penman-Monteith formulation (Monteith, 1965), E_0 is therefore parameterized as physically driven by 2-m air temperature (T). Other scalars include the

humidity – saturation (e_s) and actual (e_a) vapor pressure, the slope of the saturation vapor pressure-temperature curve at T (Δ); net radiation (R_n), soil heat flux density (G); 2-m wind speed (u_2); and the psychrometric constant (γ).

Due to the inherent difficulties in using satellite-based data (e.g., approximation of missing values due to cloud cover), remotely sensed ET products at spatial and temporal resolutions useful for drought decision-making are usually hard to obtain. Therefore, only EDDI will be used in the long-term correlation analysis to represent the demand side of the water balance (section 3.1), though both EDDI and LERI will be examined in the intra-annual case studies (section 3.2).

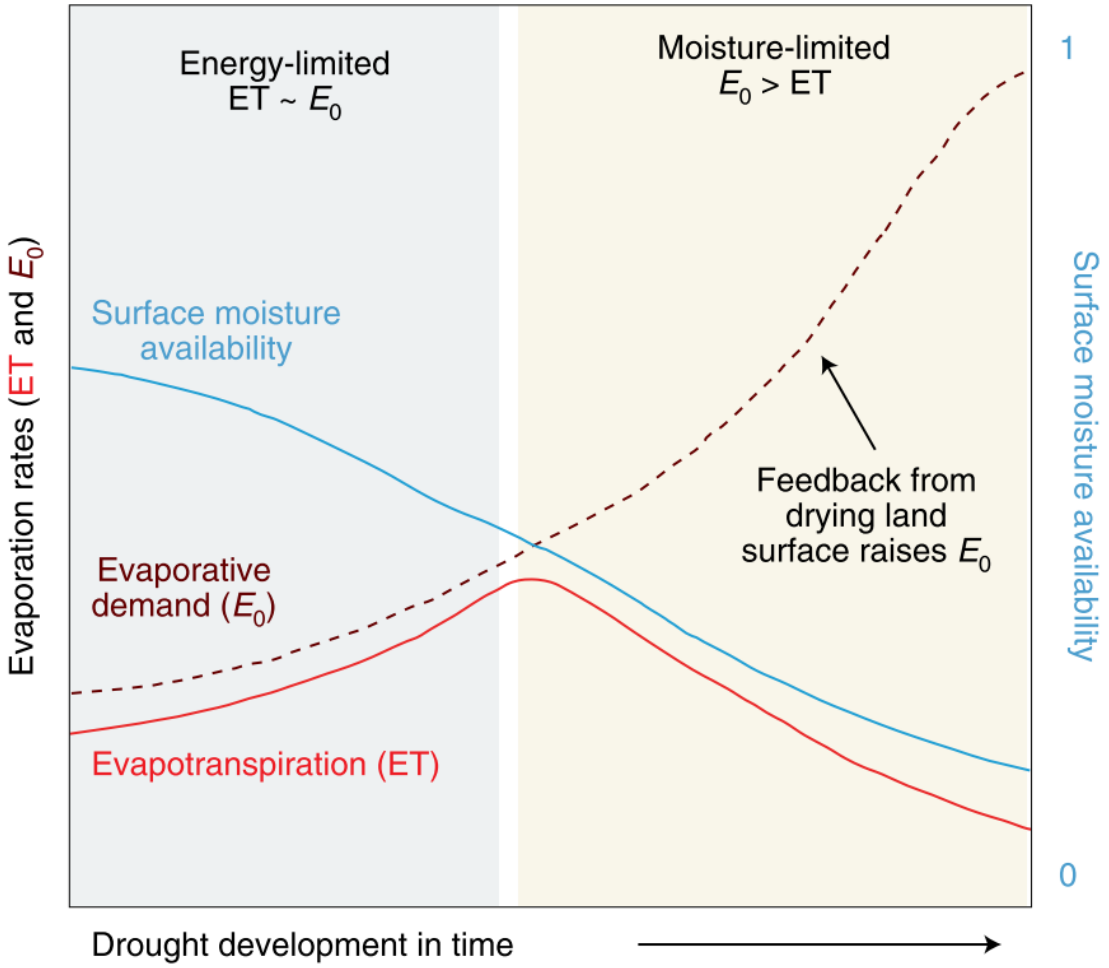

Figure 3. Conceptual representation of the Complementary Relationship (CR) between evaporative demand (E_0) and actual evapotranspiration (ET) and the schematic evolution of surface moisture availability. The farther to the right of the X-axis, the dryer the regional environment. (Adapted with permission from The EDDI User Guide – https://psl.noaa.gov/eddi/pdf/EDDI_UserGuide_v1.0.pdf)

Soil Moisture

In agricultural drought monitoring, model-based SM products often serve as the alternatives for the scarce in-situ SM observations (Robock et al., 2000). SM, together with other land surface conditions generated by the land-surface models (LSM) forced by NLDAS-2, has been widely evaluated across the CONUS (Robock et al., 2003; Schaake et al., 2004). Phase 2 of NLDAS used upgraded LSMs and better atmospheric forcings than phase 1, while extending the retrospective simulation range to 1979 through present (with a 4-day lag) (Xia et al., 2012). Noah is the primary land surface model of the Weather Research Forecast model (WRF; (Skamarock et al., 2019)) and its version 2.8 is one of the LSMs used in NLDAS-2 that generates SM products. The performance of this product across the CONUS has been comprehensively validated through intercomparison with in-situ observations and other LSMs (Cai et al., 2014; Xia et al., 2014). SM outputs from Noah-2.8 forced by NLDAS- 2 were used over the Northeast domain. The SM data has daily frequency and a period of record covering 1980-2020. The SM data are at a 1/8th-degree resolution – (i.e., 12 kms; three times coarser in length than PRCP and E_0), and available for four soil depths: 0-10 cm, 10-40 cm, 40-100 cm, and 0-100 cm.

2.1.2. Crop Datasets from The National Agricultural Statistics Service

A better understanding of the performance of drought metrics for agricultural monitoring can be gained by tracking crop conditions and production records. With most field crops being rainfed, agriculture in the Northeast is a major economic sector subject

to the vulnerability to the variation of seasonal drought. The National Agricultural Statistics Service (NASS; (USDA, 2018)), which is maintained by USDA, conducts hundreds of annual field surveys by giving questionnaires to ask farmers what, where, and when they are planting. NASS aims to publish such agricultural statistics, including crop yield and condition used in this study, to all users through censuses and surveys. Censuses provide five-yearly detailed data for the nation, each state, and some counties, while surveys are implemented at local levels at a much higher frequency through networks of state offices and universities. The crop datasets used in this study are either from or validated by these surveys.

Cropland Data Layer

The Cropland Data Layer (CDL) is a gridded, crop-specific, categorized geo-referenced product created by NASS that uses satellite imagery to generate acreage estimates for different plant categories. All historical CDL products are freely available via the Crop-Scape online tool (NASS, 2016b). For this study we extracted annual raster layers in a 30-m resolution grid for the Northeast for the period from 2009 to the present. About 90% of the pixels display a constant crop type through the period, with the primary exceptions being fields that frequently switch between two crop types. In the raster set, each land use category (crop type) was assigned a three-digit identification number as a variable. For each pixel, we arranged the identification number across the years from smallest to largest and then assigned the median value to that pixel. In this way, a single map showing the majority of crop types across the years in the Northeast was derived. Considering the number of data points (more than two billion pixels each year for the

Northeast) and our limited computing resource, we believe the median value can effectively represent the most frequently planted crop category on each pixel.

Selecting Crop Types

We focus on rainfed crops for this study to reflect natural forcing from the climate drivers that would otherwise be suppressed for irrigated crops. Based on the 2017 irrigation report published under NASS's five-yearly agricultural census (USDA, 2019), only ~13% of the farmlands were irrigated in NY during 2018, and these are generally vulnerable crops (e.g., berries, grape wineries). The irrigation coverage is even smaller for New England and PA (USDA, 2019).

According to the CDL map, in terms of land area, the top five most widely cultivated crops in the Northeast are hay, pasture, corn, soybean, and winter wheat. Based on the proportion of crop cover for six crop types in the gridMET cells (Figure 4), not only do non-alfalfa hay (hereafter referred to as hay) and pasture have the largest area coverage over other crops in the Northeast, but they also exist across a significant portion of New England. (Peña-Gallardo et al., 2019) thoroughly assessed the spatial and temporal patterns of how crop yields respond to drought across the nation (including NY and PA, but not New England) but only examined corn, soybean, and winter wheat. So, an extension to hay and pasture for the Northeast with comparison to multiple climate drivers would add value to this existing knowledge base. The results presented in this paper were focused on the yield of hay and the condition of pasture.

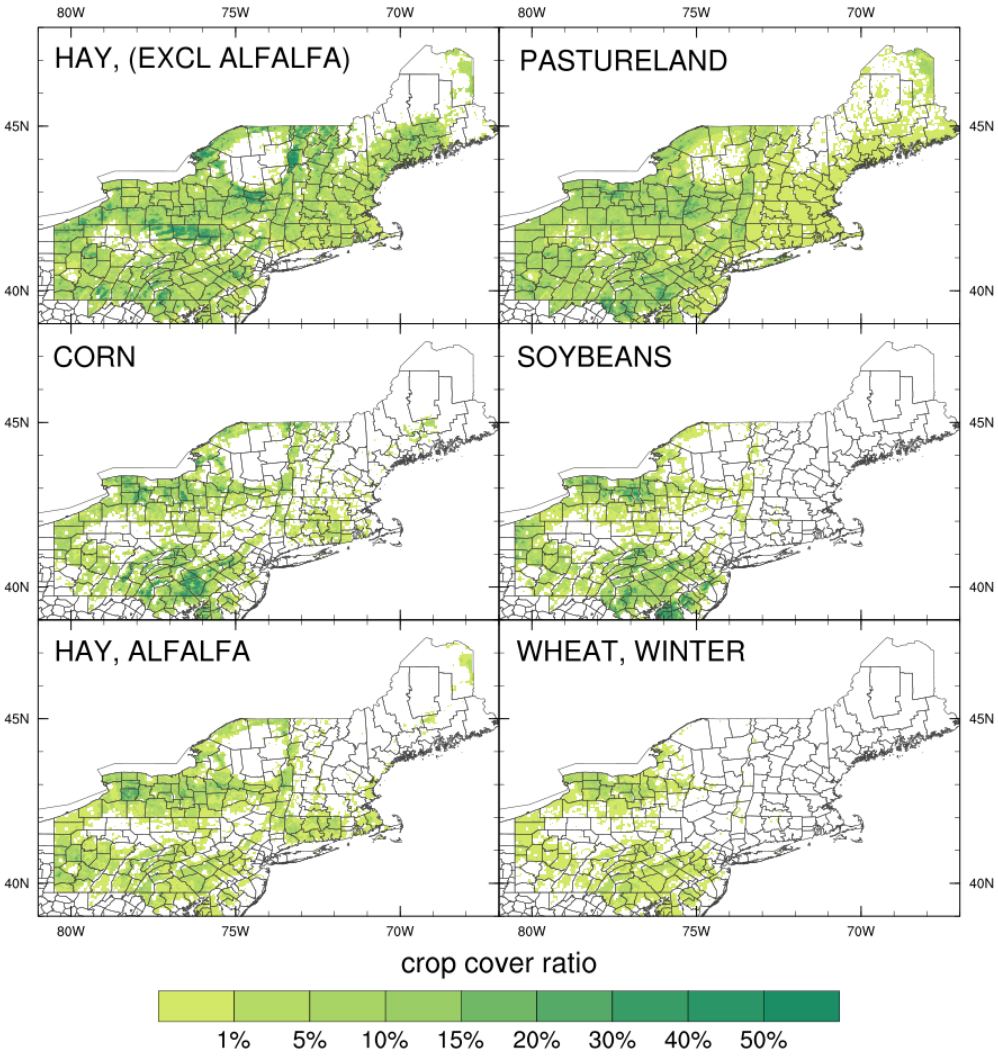

Figure 4. Crop-cover pixel ratio of gridMET cells (4 km) for the top five most widely planted (in acreage) crops in the Northeast US.

Crop Yield

Based on Figure 4, this study chose the annual yield of hay (excluding alfalfa) to represent the variability of field crop production in the Northeast from 1980 to 2020. County-level crop yield data in the Northeast US can be accessed through the Quick Stats web portal (NASS, 2016a). Given that a significant portion of the Northeast falls into land use categories other than agriculture (e.g., city, idle land, and natural reserves), the yield data in some less cultivated counties may possess much larger temporal variability than in others. Therefore, only counties with more than 1% of their land covered by hay are selected as available. Adopted from NASS, the yield data used in this study were calculated as crop production divided by harvested areas. When considering drought impact, the production per area may better reflect the capacity for producing crops as it eliminates external factors like expanded farming or anthropogenic changes in arable land area (Iizumi & Ramankutty, 2015; Wurster et al., 2020).

Detrending Time Series

Interannual variability of crop yield depends not only on climate forcing but also anthropogenic factors like evolving management strategies and farming technologies. The combination of such factors can drive a non-climatic trend in the yield data. Thus, it is necessary to eliminate these sorts of trends when examining agricultural yield in order to limit analysis to climatic factors (Lobell & Asner, 2003). After detrending, all the residuals were divided by the standard deviation of each time series to ensure states and

counties with different magnitudes of agricultural land are scaled to the same level of yield fluctuation (Potopová et al., 2016; H. Wu et al., 2004).

Crop Conditions

To track the progression of crop health within specific drought years, weekly crop conditions were extracted from NASS. NASS contacts over 3,600 respondents across the county for visual observations and subjective estimates of crop conditions (Rosales, 2021). Questionnaires from these respondents are collected weekly and aggregated to state and national levels based on NASS's acreage records, with the county-level data remaining confidential for privacy protection. Overall, data on pastureland are the most detailed of all other crop types in the Northeast. They are available weekly from April through November from 1995 for all nine states, and describe the condition as one of five categories: excellent, good, fair, poor, and very poor.

2.2. Connecting Crop Yield to Drought Indices

2.2.1. Climate-Driver Averaging and Drought-Index Derivation

Crop area-weighted Climate Drivers

As all the crop data were collected at either the state or county level, the gridded climate drivers were averaged onto these levels so that comparisons can be made. A

proper way to take the average would be to break down the grids based on the CDL-provided spatial distribution of a target crop in that state or county. The 30-m spatial resolution of the CDL is much finer than that of the 4-km gridMET variables. Therefore, the land cover proportions of specific crops in each gridMET cell can be derived based on the count of target CDL pixels, i.e., those with the desired three-digit crop-type number. For example, within the geo-referenced range of a gridMET cell, if 1200 of total 18,000 CDL pixels indicate crop type "hay," then the ratio 1200/18,000=6.67% is assigned to the gridMET cell for category "hay". In this manner, each gridMET cell was given a set of two ratio values, corresponding to hay and pasture. Then, for each county and state, a shapefile was applied to mask all the gridMET cells inside that county or state boundary with that crop type. In this case, the weighted average of PRCP and E_0 in each state and county can be derived based on the CDL. Here taking the PRCP for hay in NY as an example:

$$PRCP_{NY}^{hay} = \frac{\sum_1^n [r_i(hay) \cdot PRCP_i]}{\sum_1^n r_i(hay)} \qquad (2-2)$$

where the term on the left side indicates the state level PRCP for hay coverage in NY. On the right side, *i* represents one of the *n* gridMET cells in NY, r_i(hay) is the ratio of hay pixels (here as the target CDL pixel) over all the CDL pixels in that *i*th gridMET cell, and $PRCP_i$ is the PRCP value for that *i*th gridMET cell. By the same principle, values for other fluxes (e.g., E_0) and other target crop types can be derived. A schematic diagram is shown in Figure 5. The same applies for SM and ET except that the resolutions of grid cells for the NLDAS-2 and SSEBop models are respectively 1/8 degree and 1 km,

resulting in different CDL pixel numbers inside them. To ensure data representativeness in a way that each of these grid cells (gridMET, NLDAS-2, and SSEBop) has enough target CDL pixels, the minimum crop pixel ratio in each grid cell is set to 0.5%. For example, if the ratio of hay pixels inside a gridMET cell (in NY) is less than 0.5%, the cell won't be counted in the weighted averaging of the NY hay PRCP derived from equation (2-2).

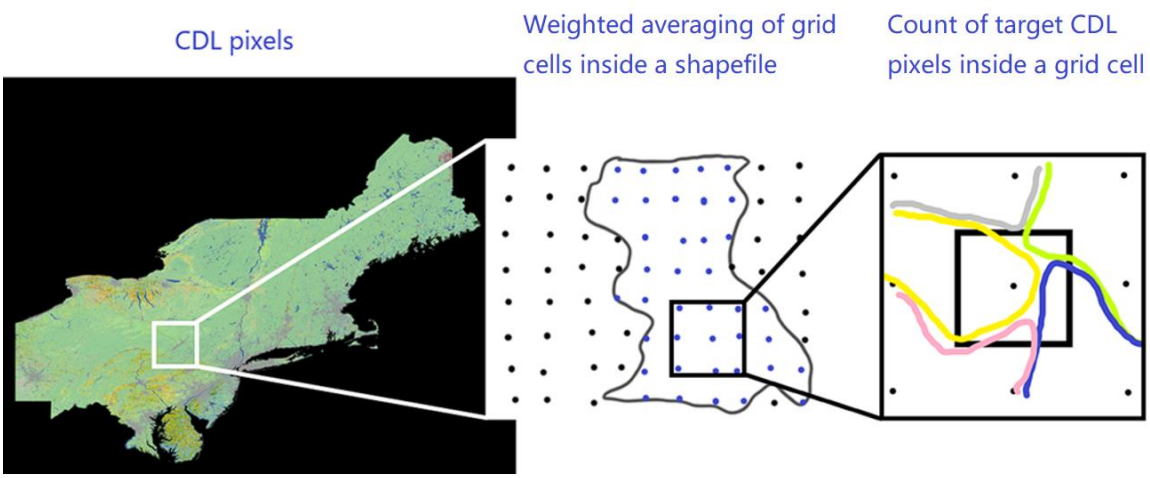

Figure 5. Schematic diagram of the crop area-weighted technique. Left: the majority of Cropland Data Layer (CDL) in the Northeast. Middle: climate driver grid cells (dot) and the shapefile of a state or county (polygon). Right: CDL pixels (areas surrounded by color curves) inside a grid cell (center square).

Calculation of Drought Indices

The drought indices used in this study are standardized scalars, with their sign indicating either dry or wet anomalies, and the offset from zero showing the severity. Positive values of SPI (more PRCP), SPEI (larger difference of PRCP over E_0), ESSMI (more SM), and LERI (higher ET) indicate wetter-than-average conditions, while negative values indicate drier. On the other hand, positive EDDI (higher E_0) means drier-than-median conditions, negative wetter. All indices standardize the anomaly in their driving flux or state using the classical inverse normal approximation (Abramowitz & Stegun, 1964). For example, an SPI of -0.5, -1.5, and -2.5 respectively indicate the probability percentiles of 30.8^{th}, 6.7^{th}, and 0.6^{th}, which means 30.8%, 6.7%, and 0.6% of the historical PRCP values are lower. However, it is their different probability distributions that separate the distinguishability of the natural phenomenon represented by these climate drivers. In most practices, PRCP records were framed into a gamma distribution to derive SPI (Naresh Kumar et al., 2009; H. Wu et al., 2005), while SPEI uses a log-logistic approach (Vicente-Serrano et al., 2010), and EDDI and LERI were based on the non-parametric empirical Tukey plotting position (Farahmand & AghaKouchak, 2015; M. T. Hobbins et al., 2016; Rangwala et al., 2019; Wilks, 2011). This study follows such methods of generating probability distribution of climate drivers to derive SPI, SPEI, EDDI. Specifically for SM, the Kernel Density Estimator (KDE; (Silverman, 2018)) method deriving of ESSMI detailed in (Carrão et al., 2016) has only been tested for South America. Since both are non-parametric empirical methods, this study replaces the KDE with Tukey plotting position in generating the SM index in the

Northeast, and names it SSMI to distinguish. As these indices are multi-scalar, they may be used to identify which timescales correspond best to different drought-impact metrics such as annual crop yield. Therefore, with the exception of LERI, all indices in this study were derived at seven timescales: 1-week, 2-week, 1-month, 3-month, 6-month, 9-month, and 1-year. For LERI, the 8-day timescale was directly used in this study after being applied to the crop area-weighting mentioned above.

2.2.2. Correlating and Mapping

The Pearson correlation coefficient (R) was used to examine how well drought indices track crop yields. Only the data points on the 1st and 16th day of each month are used in the correlation analysis to better fit the timescales shorter than one month (e.g., 1-month EDDI on May 16th indicates the E_0 anomaly from April 16th to May 15th). For hay in a desired state or county, a 40-year time series (1981-2020) for each drought index was developed (SPI, SPEI, EDDI, SSMI) with seven timescales at a twice-monthly frequency. This matrix of index time series was then respectively correlated with the time series of hay yield. A significance level of 95% (α=0.05) was used as a threshold to determine that the obtained linear relationship (i.e., R) between each pair of time series was significantly different from zero (Kendall, 1961). Based on the two-tailed t-score for a p-value of 0.05, an R of ±0.304 corresponds to a statistically significant correlation. Therefore, only areas and timescales with the |R| greater than 0.304 are presented and discussed in this study.

The strongest correlation between each drought index and hay yield in the Northeast was mapped for each county so that spatial patterns of the impact of each

climate driver on crop yield can be drawn (section 3.1.1). In addition to showing the results by polygons of state and county, the CDL layers were used to mask out areas with no crop cover to provide better visualization for states and counties with large patches of sparse crop cover. Based on Figure 4 in section 2.1.2, this study focuses on hay and pasture as they have the most coverage in the Northeast, especially in New England. For the correlation analysis, only grid cells (gridMET, NLDAS-2, and LERI) with at least 0.5% hay coverage were displayed for data representativeness. As hay is a low-volume crop in New England, county-level hay yield there is not available from NASS. Therefore, correlations were computed at the state level for New England states, but at the county level for NY, PA, and NJ. In addition to mapping the value of strongest correlations, the drought index timescale and ending month associated with those strongest correlations were also mapped.

In addition to the strongest correlations in space across the Northeast, the full distribution of timescales and ending months (e.g., 3-month SPI ending in September means the accumulation of PRCP anomalies through July, August, and September) for all correlations are shown in the form of a heat map (section 3.1.2).

2.3. Intra-annual Crop Responses to Droughts

2.3.1. Crop Score and Drought Years Identification

As noted, the pasture condition records from NASS are more detailed than for other crop types in the Northeast: they start in 2001 and include all nine states. The raw

condition data were recorded in weekly percent area in each category (e.g., according to the record, in the 28th week of 2020, pastureland across NY was by area 13% excellent, 40% good, 27% fair, 16% poor, and 4% very poor). A unified standard called Crop Score represents overall crop conditions, following the method used in the official NASS report (Rosales, 2021), repeated here:

$$Crop\ Score = \frac{(5 \times excellent + 4 \times good + 3 \times fair + 2 \times poor + very\ poor)}{100} \qquad (2-4)$$

Excellent, good, fair, poor, and very poor are each the percentage of pastureland area reported to be in that quality category. The equation yields a dimensionless value, which ranges from one to five, quantifying the weekly, statewide aggregate condition. Crop Score varies from 1, indicating all the pasturelands are "very poor," to 5 indicating all "excellent," thereby providing a comprehensive metric for the degree of pasture health.

Two recent drought events occurred in the Northeast in the growing seasons of 2016 and 2020. They are within the temporal range of all our data availability and are most relevant to the NE DEWS. These events were therefore chosen as the foci of this intra-annual case study. While the degradation of pasture conditions may illustrate the drought severity in terms of agricultural impact, the overall drought period within these two years was also verified by the USDM drought maps (section 3.2.1).

2.3.2. Time Series Comparison

For each of the nine states in the Northeast and each of the seven timescales of SPI, SPEI, EDDI, and SSMI, the time series of daily index values from March 1st to November 30th of 2016 and 2020 were compared with the Crop Score of pasture conditions within the same time frame. The weekly time series of Crop Score were linearly interpolated to a daily frequency for better visualization and comparison to daily indices. One panel diagram is generated for each state and timescale. Only the results from 1-week to 3-month timescales in MA and PA were presented in section 3.2.2 (Figures 13 to 20). Since only EDDI indicates dry when positive, the sign of EDDI was reversed to ensure that all indices below the reference line (zero) indicate drier-than-normal. The time series of eight-day LERI are only included in diagrams of the 1-week timescale, with the separate data points also linearly interpolated to daily curves. Vertical reference lines are used to stretch through the panel diagrams to highlight such correspondences. The other main purpose of the time series comparison is to determine which timescale the dry period shown by each drought index correlates most strongly with pastureland degradation (declining Crop Score). In this manner we identify the most appropriate timescale of each climate driver regarding its agricultural drought impact in the Northeast.

3. Results

3.1. Correlation Analysis

3.1.1. Strongest Correlation and Timing

Strongest Correlation Map

Figure 6 showed the strongest R (hereafter referred to as R_{max}) between hay yield and drought indices at the county level in NY, PA, and NJ, while at the state level for New England states. As followed by other figures in section 3.1, panel a), c), and e) represent, respectively, SPI, SPEI, and EDDI, while panel b), d), and f) represent three layers of SSMI.

SPI (Figure 6a) generally showed positive R_{max} across PA, the west half of NY, and the southern New England states. Several counties in central-western NY, western PA, and central-eastern PA showed values of R_{max} greater than 0.6, and almost all other PA and western NY counties showed positive R_{max} between 0.4 and 0.6. However, for counties immediately north and south of the Adirondack Mountains, negative R_{max} were found with some passing -0.5. Additionally, several counties along the Hudson River Watershed (southeastern NY and northern NJ) also showed negative R_{max} (-0.5). For New England states, positive R_{max} exceeding 0.5 were shown for MA and CT, while weak negative R_{max} were found for RI and ME.

The R_{max} for SPEI indicates the connection between hay yield and the difference of PRCP minus E_0, instead of PRCP alone. However, the spatial pattern of R_{max} in the map for SPEI (Figure 6c) was still similar to that of SPI. For example, counties with R_{max} greater than 0.6 were also shown in western NY, western PA, and central-eastern PA. This similarity also applies to counties with negative R_{max} in eastern NY and northern NJ. For New England states, the spatial pattern of R_{max} for SPEI was even closer to that for SPI, except for NH, in which R_{max} switched from weakly positive (0.3 to 0.4) to weakly negative (-0.3 to 0.4).

On the other hand, EDDI has mostly negative values of R_{max} (Figure 6e) across the region, as higher E_0 usually leads to lower yield in the presence of drought. Several counties in western PA and northwestern NJ showed R_{max} lower than -0.6. Only scattered counties in NY and southern PA showed positive R_{max} for EDDI. An area that consistently showed positive R_{max} could be found in central-western NY, where five counties are distinct from the surroundings. For New England, R_{max} for EDDI showed weakly negative (-0.3 to -0.5) in most states, with the exceptions of CT and NH, which showed positive.

The R_{max} maps for all three depths of SSMI (Figure 6b, 6d, 6f) also showed similar spatial patterns as for SPI, with more positive and stronger R_{max} values found in the surface layers. With positive correlation implying that higher SM leads to more hay yield, large areas of positive R_{max} were shown by all three depth layers in western NY, PA, and western NJ. Negative R_{max} can be found in eastern NY and northern NJ. For the surface layer (0-10cm, Figure 6b), only three counties in western NY and four in PA

show negative R_{max}. For the middle layer (10-40cm, Figure 6d), more counties in central NY started to show negative R_{max}. For the deep layer (40-100cm, Figure 6f), more western and central NY counties showed negative R_{max}, with the central-northern PA also switched to negative. Despite these areas, the spatial pattern of R_{max} had a good consistency between the three depths across NY, PA, and NJ. For counties with such consistency, the magnitude of R_{max} in the surface layer was slightly larger than in the deep layer. In New England, The R_{max} for the surface layer SSMI showed positive for all available states ($|R_{max}| < 0.304$ in ME being insignificant). The same pattern applied for the middle layer, except that VT became insignificant. However, the R_{max} map for the deep layer in New England was quite different from the upper layers: R_{max} for CT increased to over 0.5; in MA it dropped below 0.5; in VT it switched to weakly negative (-0.3 to -0.4); in NH it became insignificant; and in ME it became weakly positive (0.3 to 0.4). In general, R_{max} values at the state level in New England were lower than at the county level in NY, PA, and NJ. Since most states in New England are much larger than counties, it is still unclear whether such weaker R_{max} values are caused by the inherent weaker connection between hay and the climate or the averaging of hay yield over a larger group (county vs. state).

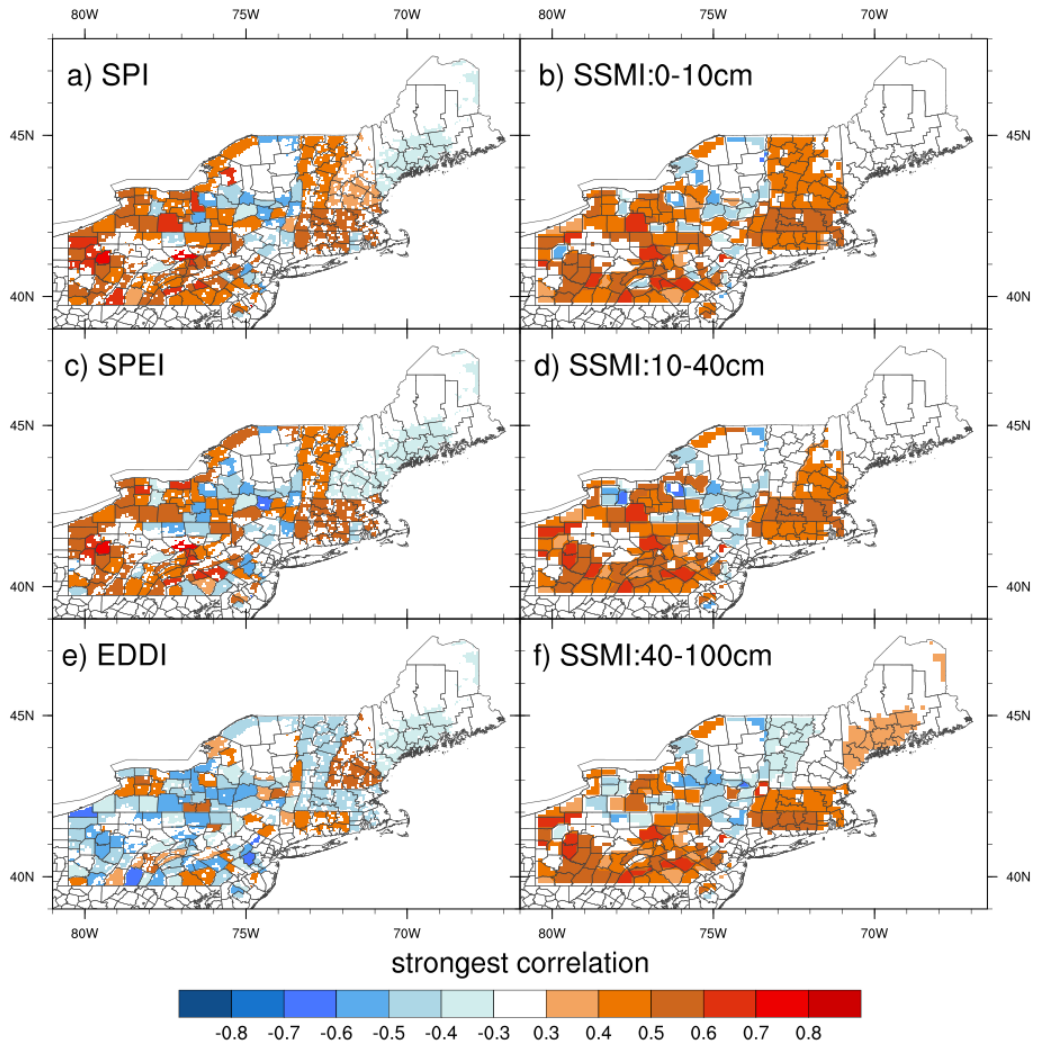

Figure 6. Strongest correlations (R_{max}) between hay yield and drought indices at the county level in New York, Pennsylvania, and New Jersey, while at the state level for New England states.

Timescales and Ending Months of the Strongest Correlations

Figure 7 and Figure 8, respectively, showed the timescales and ending months of the drought indices associated with the R_{max} in Figure 6. In general, timescales and ending months associated with the R_{max} exhibited strong spatial variability across the Northeast. In summary for all indices, two critical time windows were identified, with the timescales of R_{max} for EDDI shorter than for others. One is the mid to late summer months (e.g., 1-week to 1-month timescales ending in July, 3-month timescales ending in August and September, and 3- to 6-month timescales ending in November and December), hereafter called the "late-summer type"; the other one is the mid spring months (e.g., 1- to 2-week timescales ending in April and 1- to 3-month timescales ending in June) – the "mid-spring type". In addition, a few counties and states across the region had their R_{max} associated with the winter or even fall of the previous year – the "winter type".

These three types were prominently shown in NY, PA, and NJ at the county level. For R_{max} regarding SPI (Figures 7a and 8a), most PA counties with 1-week to 1-month timescales had their ending months in the summer. The only exceptions are the counties in the northeast corner of PA, which ended in September and December. PA counties with 3- to 6-month timescales generally had their ending month in the fall or December. For western NY, most counties showed 1- to 3-month timescales ending in the summer. Some counties in central-northern PA, eastern NY, and western NJ showed 1-week to 1-month timescales ending in the spring. Additionally, a small number of scattered counties across the region showed 1-week to 6-month timescale ending in January and February.

For R_{max} regarding SPEI (Figures 7c and 8c), the patterns were similar to what the SPI map showed, except that some counties had longer timescales ending in later months of the year. For R_{max} regarding EDDI (Figures 7e and 8e), almost all counties across the region have shorter timescales than for SPI and SPEI. Most PA counties showed 1- to 2-week timescales ending in the summer and fall. The same situation applies for NY, except that multiple western NY counties started to show 1- to 2-week timescales ending in the spring. Patterns in the surface SSMI map (Figures 7b and 8b) were similar to those in the SPI map, except that some eastern NY counties changed from spring into 1-week timescales to 1-month timescales ending in November. Another difference is that several adjacent counties in the southeastern corner of PA changed to ending in January and February. The mid-layer SSMI map (Figures 7d and 8d) is similar to the patterns of the surface layer, with several western PA counties changing from 1- to 3-month timescales ending in November to 3- to 6-month timescales ending in December, while the timescales for a few counties across NY ended in the preceding winter. For the deep soil layer (Figures 7f and 8f), more counties along the border of NY and PA changed from ending in summer to ending in spring.

The three types of combination of timescales and ending months of drought indices associated with R_{max} can also be found for New England states (also included in Table 1). For R_{max} regarding SPI and SPEI (Figures 7a, 8a, 7c, and 8c), the late-summer type generally applies in CT, MA, and NH, while the mid-spring type applies in ME and VT. The only exception is SPEI in NH (9-month timescale ending in April), given the associated R_{max} being almost insignificant (R_{max} = -0.35). For R_{max} regarding EDDI, the

late-summer type applies in ME, the mid-spring type applies in MA, and the winter type applies in CT and NH. For R_{max} regarding SSMI, states with significant R_{max} generally were in the late-summer type. Additionally, results in RI were significantly different from other states, likely due to its small area and potential impacts from the urban climate or other local factors. In summary, timescales and ending months associated with R_{max} in the New England states span the entire year depending on the index and state. Among the indices, EDDI showed completely different results from the others. Across the states, the New England states, especially ME and VT, showed more variable results than the others.

Table 1 shows the R_{max} for SPI, SPEI, EDDI, and middle layer SSMI at each state level with the associated timescale and ending month. Correlation coefficients of $|R| < 0.304$ were discarded due to the 95% significance level filter. Only the 10-40 cm SSMI is shown, representing the main portion of the effective root-zone depth of hay (Efetha et al., 2009; Irmak et al., 2007). Generally, the mid-spring and late-summer types mentioned above can be found for all four indices in most states, with EDDI showing shorter timescales than other indices for each type. The results shown for SPEI generally agreed with those shown for SPI except in NH, where both SPEI and SPI had R_{max} values close to ±0.304 (around ±0.35). Additionally, the winter type was found for EDDI in CT and NH with timescales longer than six months.

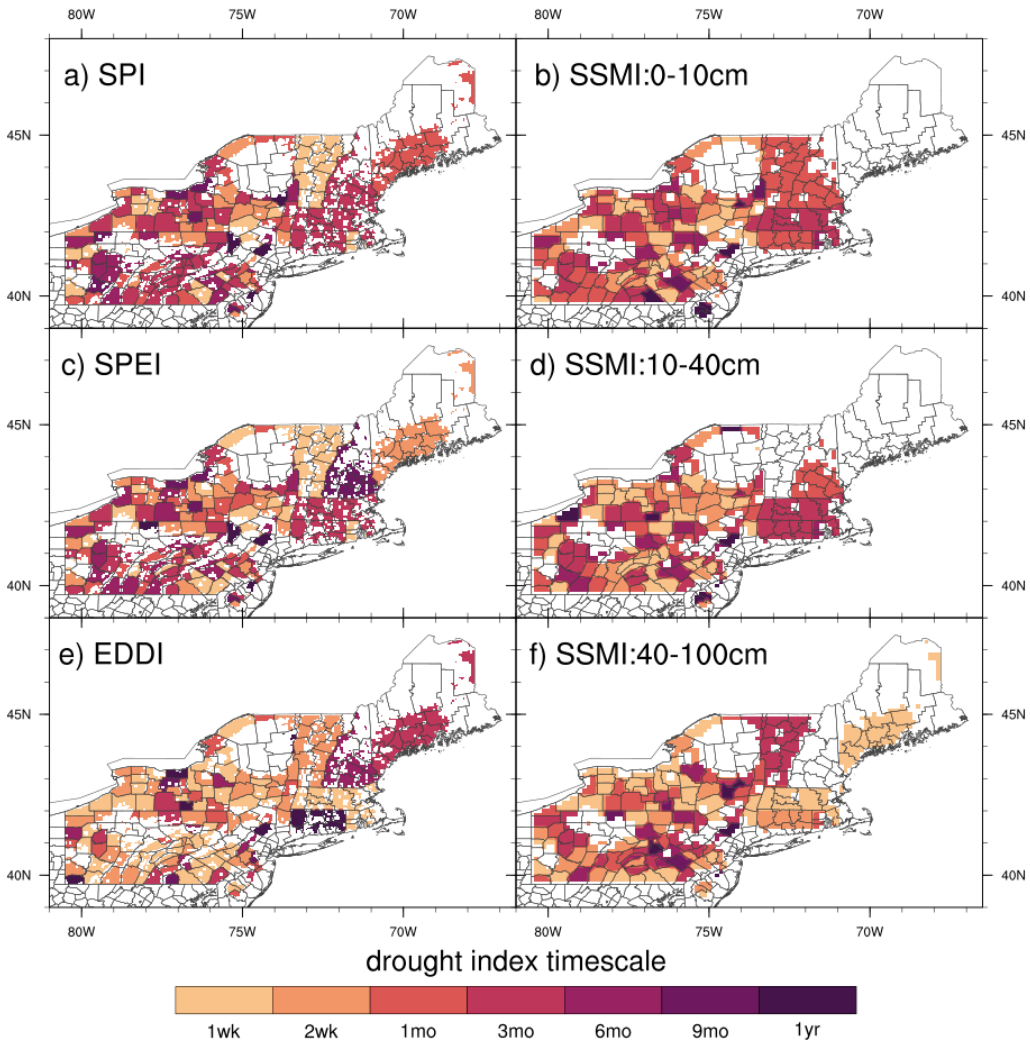

Figure 7. The associated timescale of the strongest correlations (R_{max}) between hay yield and drought indices at the county level in New York, Pennsylvania, and New Jersey, while at the state level for New England states.

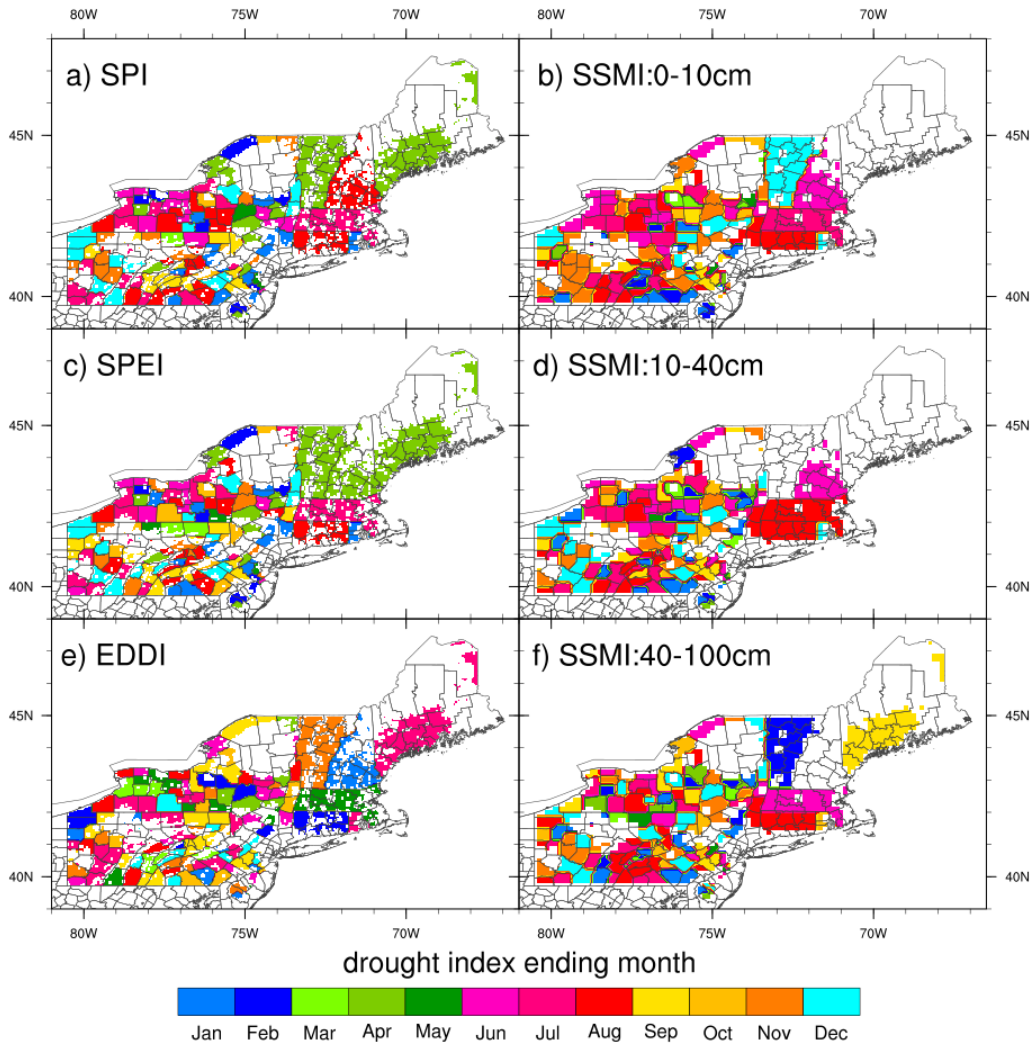

Figure 8. The associated ending month of the strongest correlations (R_{max}) between hay yield and drought indices at the county level in New York, Pennsylvania, and New Jersey, while at the state level for New England states. Ending months were separated into colors of winter (blues), spring (greens), summer (reds), and fall (yellows)

	SPI			SPEI			EDDI			SSMI (10-40cm)		
	R_{max}	TS	MON	R_{max}	TS	MON	R_{max}	TS	MON	R_{max}	TS	MON
CT	0.54	3mo	AUG	0.53	3mo	AUG	0.49	1yr	FEB	0.48	3mo	AUG
ME	-0.39	1mo	APR	-0.39	2wk	APR	-0.38	3mo	JUL	0.295*	2wk	SEP
MA	0.60	3mo	JUL	0.59	3mo	JUL	-0.42	1wk	MAY	0.51	3mo	AUG
NH	0.36	3mo	AUG	-0.35	9mo	APR	0.58	6mo	JAN	0.42	1mo	JUN
NJ	0.36	3mo	AUG	-0.35	2wk	AUG	-0.36	2wk	AUG	0.35	3mo	SEP
NY	0.45	1wk	APR	0.47	1wk	APR	-0.40	3mo	DEC	0.49	6mo	SEP
PA	0.60	3mo	AUG	0.57	1mo	JUL	-0.47	2wk	SEP	0.58	3mo	SEP
RI	-0.45	1wk	JAN	-0.46	1wk	JAN	-0.47	1wk	JUL	0.43	6mo	DEC
VT	0.43	1wk	APR	0.40	1wk	APR	-0.46	2wk	NOV	0.3038*	2wk	MAY

Table 1. The associated timescale (TS) and ending month (MON) of the strongest correlation (R_{max}) between hay yield and SPI, SPEI, EDDI, and SSMI (10-40cm) at each state level in the Northeast. Insignificant R_{max} ($|R_{max}| < 0.304$, outside the 95% significance level) were marked by *.

3.1.2. Insight from Full Distribution of Correlations

Aside from the R_{max}, the distribution for a given spatial extent (i.e., state or county) of all correlations amongst different ending months and timescales can also provide useful information. The relative importance of how each combination of "timescale + ending month" compared to one another was visualized by this distribution. Suppose a correlation is stronger than its adjacent correlations in this distribution matrix (shown by tiles with deeper colors than their surroundings in Figures 9 and 10). The combination associated with this correlation is referred to as the "PEAK" in this paper. In Figures 9 and 10, the X and Y axes of each panel respectively represent the ending month and timescale, while shading in the heat maps indicates the sign and strength of the associated correlation. Only results at the state level for MA and PA were presented in this section, as signals for the other states either conveyed similar information or were too weak to show distinguishing features.

Figure 9 shows the distribution of correlations between drought indices at various timescales and ending months and hay yield in MA. The correlation reflects the overall characteristics of statewide hay yield responding to drought indices. In coincidence with the R_{max}, the PEAKs generally identified three periods in the year – mid-spring, late-summer, and the preceding winter, with the signal around late-summer being significantly stronger than the other two. Three areas of strong correlations were found for SPI (Figure 9a): positive PEAKs for the 3-month timescale ending in July; the 1-year timescale ending in around July; and a negative PEAK for the 1-week to 1-month timescales ending in October. For the July-ending 3-month PEAK, the surrounding color

tiles tended to tilt to the right by showing 1- to 2-week timescales ending in June through the 6-month timescale ending in September, by which all pointed to some dates in around June and July. The distribution of correlation for SPEI (Figure 9c) was similar to that for SPI, except that the correlations for the 1- to 2-week timescales ending in June were slightly weaker. However, the correlation distribution for EDDI (Figure 9e) showed opposite signs from that of SPI and SPEI with similar PEAK positions. Three PEAKs were identified for EDDI: a negative correlation for the 1-week timescale ending in May and the 3-month timescale ending in July, but a positive correlation for the 1-week timescale ending in October. Additionally, EDDI did not show any correlation at the longer timescales (for the 1-year timescale ending around July, as shown by SPI and SPEI). In May and October, the PEAKs for EDDI were at shorter timescales than for SPI and SPEI (1-week vs. 1-month). All the distributions for SSMI (Figure 9b, 9d, and 9f) generally had their positive PEAKs at the 3-month timescale ending in July and the 1-month timescale ending in June. Again, long timescales (9-month to 1-year timescales) were not shown by the SSMI.

Figure 10 shows the distribution of correlations between drought indices and hay yield in PA. The distribution heat maps indicated that correlations throughout the year in PA are generally stronger than in MA, with the position of PEAKs being similar. The largest positive PEAK for SPI (Figure 10a) was in the summer for a 1-month timescale ending in July to a 3-month timescale ending in September. Two other positive PEAKs, which could be seen as the extension of the largest PEAK, appeared for the 6-month timescale ending in November and the 9-month timescale ending in December. In

addition, a weak positive PEAK can also be identified for the 3-month timescale ending in January. Lastly, a weak negative PEAK was shown for the 1-month timescale ending in April. The correlation distribution for SPEI (Figure 10c) exhibited almost identical characteristics to those shown by SPI. The correlation distribution for EDDI (Figure 10e) only showed a weak negative value in the summer with the same type of right-tilted shape as mentioned for SPI. The negative PEAK of EDDI is seen at the 1-week to 1-month timescales ending in September, a point at which SPI and SPEI PEAK had longer timescales (3 months). The correlation distributions for the surface- and mid-layer SSMI (Figure 10b and 10d) were similar, generally following those of SPI, except that the positive correlation ending in January had a wider range of timescales (1-week to 6-month); no correlation was shown for long timescales (9-month to 1-year) in the summer; no negative correlation was shown in April. Compared to the above, the deep-layer SSMI (Figure 10f) lost the correlation in January and gained some at long timescales in the later months of the year (September through December). Another feature of all the SSMI heat maps is that no signal was shown for 1- to 3-month timescales ending in around October. Other than that, the same timescales in September and November both had positive correlations.

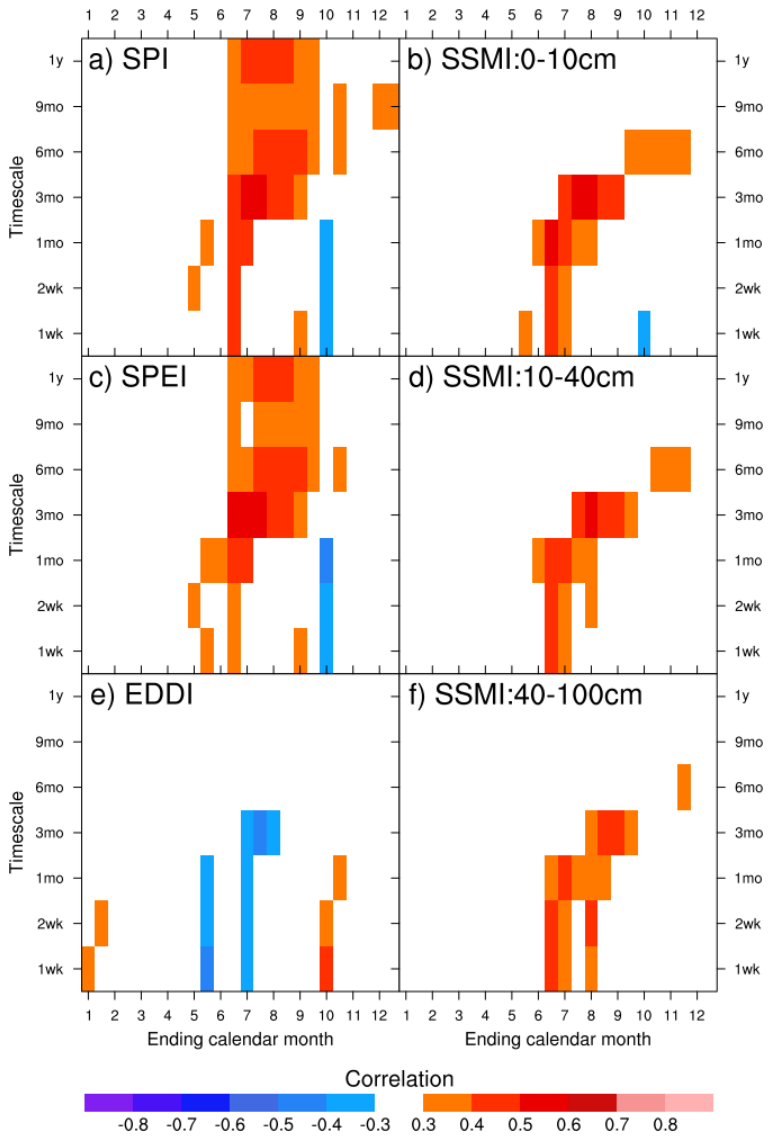

Figure 9. Distribution of correlations between hay yield and drought indices in Massachusetts, tiled by timescales (y-axis) and ending months (x-axis). Colors indicate the correlation (R) associated with the timescale and ending month.

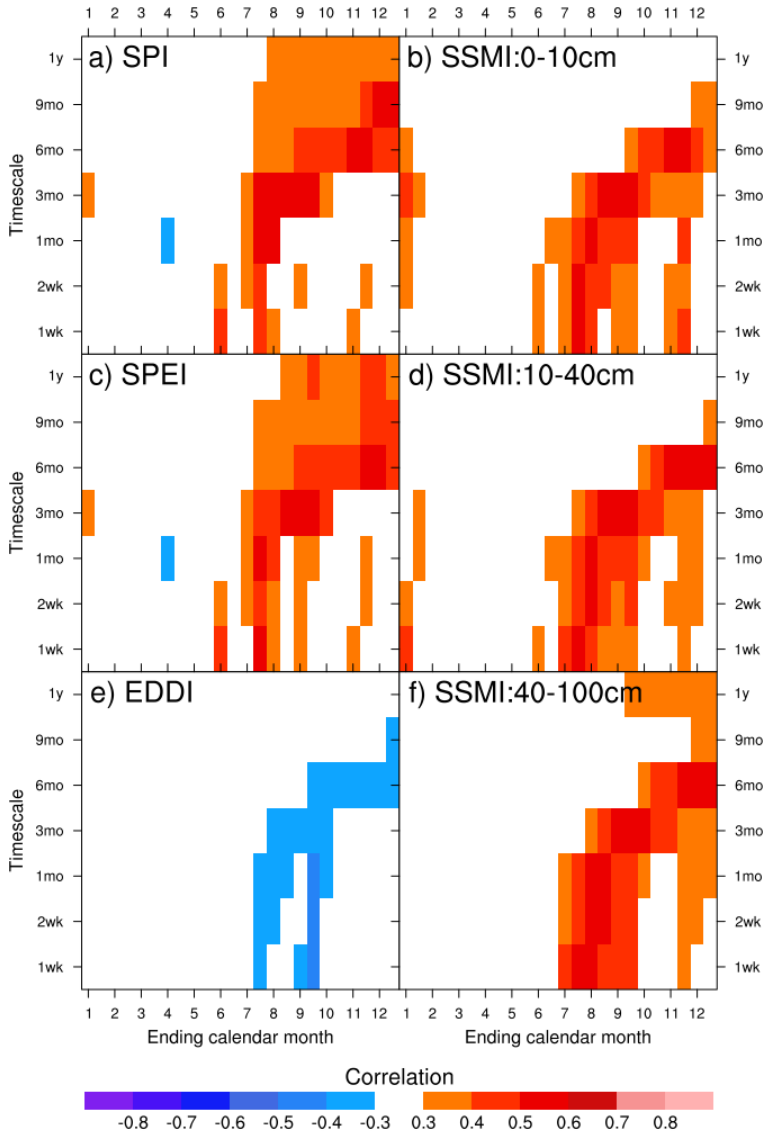

Figure 10. Distribution of correlations between hay yield and drought indices in Pennsylvania, tiled by timescales (y-axis) and ending months (x-axis). Colors indicate the correlation (R) associated with the timescale and ending month.

3.2. Case Study of Recent Drought Years

3.2.1. Drought and Pasture Conditions in Selected Years

2016 and 2020 were selected as case study years based on the drought-category maps and time series for the Northeast Climate Region from the USDM. USDM is a collection of maps released weekly showing the existing drought conditions across the US. Considered the “national drought man”, USDM relies on drought-relevant communities across the US to synthesize and interpret data from various numeric sources (Svoboda et al., 2002). It takes a convergence-of-evidence approach on a wide range of indicators, including, but not limited to, drought indices, remotely sensed vegetation and SM, streamflow and snowpack records. Drought severity in the USDM is categorized into five levels, from abnormally (D0) to exceptionally (D4) dry. As in each member of the blend of drought indicators, the corresponding percentile for each level is 30-21 (D0; abnormally dry), 20-11 (D1; moderate drought), 10-6 (D2; severe drought), 5-3 (D3; extreme drought), and 2-0 (D4; exceptional drought). Maintained by the National Drought Mitigation Center (NDMC), the archived record starts in 2000 and is downloadable in various forms (https://droughtmonitor.unl.edu/Maps.aspx).

The 20-year drought time series in the Northeast suggests that 2016 and 2020 as significant drought years. As summarized in Figure 11, despite the multi-year drying that occurred in the early years of this century, 2016 and 2020 were highlighted by >20% of the area in drought category D2 in summer and fall. The weeks ending 09/27/2016 and

10/13/2020 were the two periods when the respective droughts reached their peaks in terms of area in each drought category. Spatially, a large portion of the Northeast was estimated to be at least abnormally dry (D0) in those weeks. During the week ending 09/27/2016, central PA, western NY, southern ME, and all southern New England were under severe drought (D2), with western NY and coastal New England experiencing extreme drought (D3). In the week of 10/13/2020, the situation was slightly better for NY and PA but much worse for New England: NH, MA, CT, and RI had larger areas above D2 than in 2016, and all of ME was above moderate drought (D1) with scattered D3. We therefore examined 2016 and 2020 to show the agricultural impact of various climate drivers for the growing season droughts.

The progression of pasture conditions scores for each year between 1995 and 2020 is shown in Figure 12. For CT (Figure 12a), ME (Figure 12b), MA (Figure 12c), NH (Figure 12d), PA (Figure 12g), and RI (Figure 12h), the curves for 2016 and 2020 shared a typical shape: a normal spring followed by severe deterioration in the summer then slight improvement in the fall. This is particularly evident in MA, where, in 2016, the condition started from average in spring then quickly dropped below other years in the summer. Despite the improvement after September, the condition at the end of 2016 was the worst among all years. This pattern was also found for 2016 in CT and both years (2016 and 2020) in NH, PA, and RI, except that there were milder degradation and worse years around 2000 in PA. For 2020 in MA, the condition started below average but had an improvement in the summer, after which it declined sharply, becoming the worst by early fall. Such a pattern was also found for 2020 in CT and both years (2016 and 2020)

in ME. On the other hand, in NJ (Figure 12e), 2016 and 2020 were no worse than other years. In NY (Figure 12f), the pasture conditions for 2016 did not deteriorate significantly. In VT (figure 12i), the pasture conditions for 2020 was consistently better than the other years.

MA was chosen as the state for the time series comparison considering the above representativeness in pasture conditions patterns during 2016 and 2020 and the fact that it has a higher hay R_{max} than other New England states (section 3.1.1). Similarly, PA was also chosen due to its temporal patterns for pasture conditions, hay R_{max}, and size and location (away from New England).

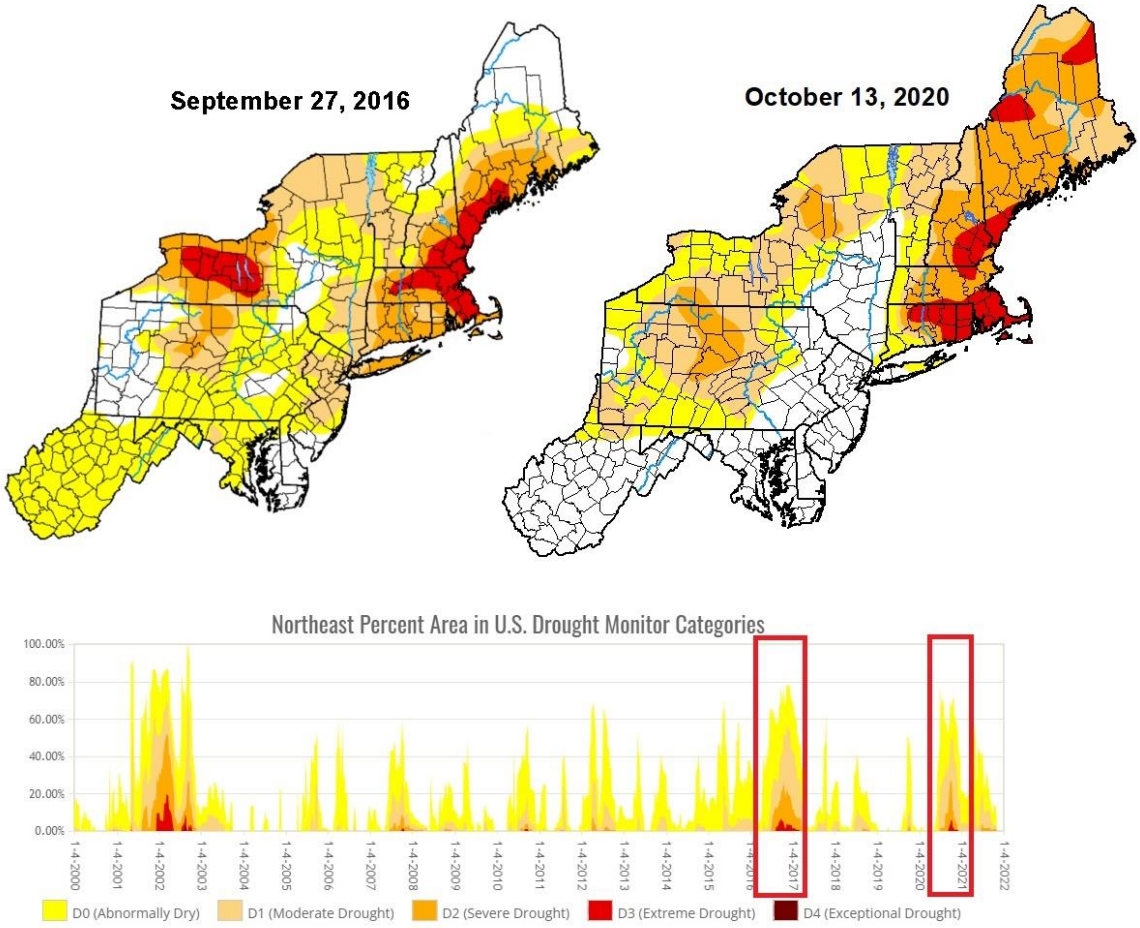

Figure 11. (Top) USDM maps for the weeks ending 09/27/2016 and 10/13/2020, and (bottom) 2000 to 2021 time series of areas covered by each USDM drought category across the Northeast Climate Region. The 2016 and 2020 droughts were highlighted in red boxes. Adapted from the United States Drought Monitor (https://droughtmonitor.unl.edu/).

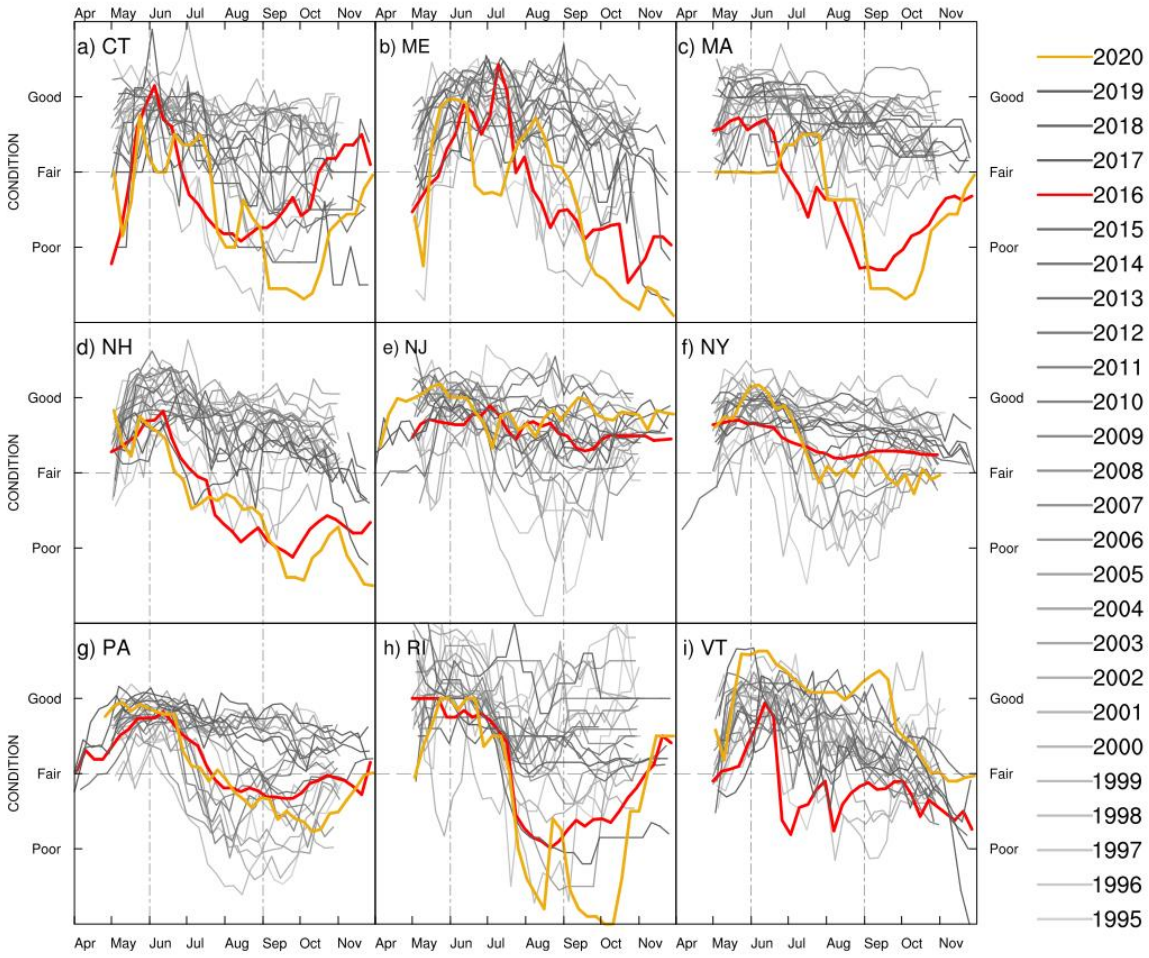

Figure 12. Progression of state level weekly pasture conditions scores during the growing seasons of 1995-2020 in the Northeast. 2016 and 2020 were highlighted using red and yellow lines, respectively.

3.2.2. Time Series Comparison

The temporal distribution of correlations shown in Section 3.1.2 generally reflected the significant timescales of drought indices that potentially affect crop yield in the Northeast. However, a detailed comparison of the correlation of crop conditions to different indices during drought episodes is still needed to extract the most suitable timescale for each crop/timescale combination. In addition, the evolution of and interaction between drought indices during drought events could be revealed through a daily or weekly time series analysis.

Massachusetts

Figures 13-16 demonstrated the effects of increasing timescale on the responsiveness of pasture conditions to the drought indices in MA during the growing seasons of 2016 and 2020. Notably, as the timescale increases, the drought indices that pasture conditions responded to most are, in order, SSMI, EDDI, then SPI.

Figure 13 shows the progression of 1-week drought indices and statewide pasture conditions. The Y-axis for EDDI was reversed to make all indices above the reference line indicate wet and below indicate dry. The most widely planted pasture species in the Northeast are Kentucky bluegrass, tall fescue, orchard grass, and white clover (Goslee & Gonet, 2018). Their potential root depths range from 40 cm to over 100 cm (Bush et al., 2012; Evans, 1978; Lin, 1985). However, the effective root zone of pasture is typically one to two thirds of the deepest roots (Lacey, 2019). Thus, in this case, only the SSMI at the 10-40cm depth was shown.

Indices at the 1-week timescale generally fluctuate in a period of two weeks, reflecting the successive wetting and drying at the synoptic scale. In 2016, the area experienced two strong PRCP events (SPI above 1.0) in the spring, several weak wetting events (SPI around 0.5) in the summer, and a series of moderate wetting events (SPI ranging from 0.3 to 1.0) in the fall. In between these wetting events were dry periods highlighted by very low SPI (around -1.5) and high EDDI (greater than 1.5). Since SPI and EDDI showed the same drought signal (both showing wetting or drying) throughout most of 2016, the fluctuation of SPEI followed them well though tracking closer to SPI. There are several periods when SPI and EDDI showed disagreement (mostly normal SPI with high positive EDDI) as the SPEI tracked closer to SPI (late May, early July, mid August, and late October). From the SSMI trace, we see that the area's SM started low (SSMI below -1.5) in the early spring but later recovered due to the two wetting events. The fluctuation of SSMI after March followed SPI and SPEI, though lagging by about one week. SSMI also showed a delayed response to SPI and SPEI regarding the amount of moisture. As a result of drying in late June, SSMI dropped below -2.0. However, with positive SPI and extremely weak E_0 (EDDI less than -2.0) in early July, SSMI could not switch to positive before the next drying in late July. The same situation applied for August which eventually made SSMI remain negative until late October. For LERI, its fluctuation strictly followed the variation of SSMI before mid August. After that, little correspondence was observed between LERI and other indices. The pasture conditions started as good in the spring then had two major degradation events in the summer. Both events were accompanied by pre-existing SM deficits signaled by low SSMI. Further, the periods of degradation also overlapped with those of normal SPI and extra positive EDDI

and were accompanied by minimal values of LERI. In the fall, the condition experienced a slow recovery despite negative SSMI, however with positive SPI and LERI (we consider the 0 percentile LERI in April and October as invalid data points).

Similarly, in 2020, a number of wetting processes throughout the year were separated by slightly longer drying periods, as shown by SPI and EDDI. Despite the strong wetting events in the spring and fall, SSMI remained below normal for most of the time from mid May to early October. The only exception was at the end of June, when SSMI became briefly positive, due to a strong wetting event. This short period was also accompanied by a recovery in LERI and in the pasture conditions. Again, SPEI better followed the variation of SPI than the other indices for the entire year; LERI only followed SSMI before August. The two major degradations of pasture matched the pre-existing low SSMI (late July and late August). The late July degradation coincides with the disagreement between SPI (slightly wet signal) and EDDI (dry signal) that was accompanied by below-normal SSMI and low LERI. Given such degradations, the pasture conditions eventually recovered due to a strong wetting period in October.

Figure 14 shows the progression of drought indices at the 2-week timescale. Compared to the 1-week time series, the dry and wet periods throughout the growing seasons of 2016 and 2020 can be more clearly identified with fewer drastic oscillations. Only three moderate wet periods are evident in 2016 (early April, early May, and October), four in 2020 (late March through early May, early July, early September, and mid October through mid November). Between these wetting periods were strong dry periods. As a result, almost every dry period caused the SSMI to decrease below -2.0

while each of the wet processes did not bring the SSMI above zero. SSMI correlates well with pastureland degradation from early summer through fall. However, SM deficits in the late spring seemed to have little effect on pasture health. For SPI and EDDI, periods of disagreement can also be identified at this timescale (e.g., mid August 2016 and late August 2020), when SPI showed near-normal PRCP and EDDI showed strong E_0. In both periods, the SSMI were under recovery while the pastureland experienced major degradation. On the other hand, late April 2016, late May 2016, and late June 2020 are three dry periods when SPI showed strong PRCP deficit (SPI below -1.5) while EDDI showed moderate E_0 (EDDI less than 1.0). Pasture conditions did not change significantly during these periods.

Figure 15 shows the progression of the 1-month drought indices in MA during the 2016 and 2020 droughts. The curves were slightly flattened with the dry and wet periods showing prolonged features. All periods when pastureland experienced degradation (summer 2016 and late summer 2020) can be correlated with drier-than-normal SPI and EDDI. Again, EDDI showed slightly better correspondence than SPI. In May 2016, when EDDI showed a wet signal while SPI showed dry, the condition did not change much. In August 2016, when EDDI showed a strong dry signal while SPI was near normal, pasture conditions degraded significantly. Another feature evident at this timescale is that SSMI appears to have lost its role in determining pasture conditions. SSMI remained below -1.0 throughout most of 2016, but pasture conditions only started dropping after mid June. Additionally, the SSMI, which was consistently below -2.0 in June 2020, could not explain the short-lived, simultaneous improvement of pasture conditions.

Figure 16 shows the progression of 3-month drought indices across MA during the 2016 and 2020 droughts. At this timescale, all indices are further flattened relative to their 1- and 2-week and 1-month counterparts. SSMI at this timescale (remained below -1.0 throughout both years) appears to have lost relationship to the timing of pastureland degradation. However, for SPI and EDDI, the curves generally match to pasture conditions. Two small discrepancies are evident in the EDDI time series: in early summer 2016 pasture conditions dropped while EDDI was near-normal; and in late fall 2020 pasture conditions improved while EDDI remained greater than 2.0. By contrast, the curve of SPI at this timescale matches pasture conditions much more closely. Almost every time once SPI dropped below -1.0 (late June 2016, late July 2020), pasture conditions also dropped. Once SPI increased above -1.0, pasture conditions either stopped degrading or improved. The time series of indices at the 6-month and longer timescales were also investigated in this study. However, due to the nature of the 2016 and 2020 droughts, curves of these longer timescales turned out to be persistently below the zero-reference line and were flattened to such a degree that they demonstrated few variations. Therefore, their value in comparison to the change in pasture conditions were lost and are thus not presented here.

Pennsylvania

Figures 17-20 demonstrated the effects of increasing timescale on the responsiveness of pasture conditions to the drought indices in PA during the growing seasons of 2016 and 2020. The sequence of timescales of each drought index to which

pasture conditions responded most was similar as in MA – from shorter to longer timescales: SSMI, EDDI, then SPI.

Figure 17 shows the progression of 1-week drought indices and pasture conditions in PA during the growing seasons of 2016 and 2020. Similar to the results for MA, indices at this timescale fluctuate in periods of two weeks, alternating between wetting and drying at the synoptic scale. Both years experienced a strong wetting event (SPI above 1.0) in late spring accompanied by weak E_0 (EDDI less than -1.0), which increased the below-normal SSMI to a maximal value (0.5 for 2016 and 2.0 for 2020) in early May. However, SM in both years was soon depleted by the drying in late May, resulting in a negative SSMI throughout both summers. Despite several strong wetting events (early July 2016, early August 2016, mid August 2016, mid July 2020, and early August 2020) in both years, E_0 remained above normal (EDDI greater than 0) throughout the summers. In the fall of both years, another wave of drying turned SSMI negative into the winter. Similar to MA, the progression of SPEI in both years showed a closer match to SPI than to EDDI. For LERI, an almost synchronized variation of LERI and SSMI can be found from early May to late September. This correlation was limited to early June to early September. For pasture conditions, periods of degradation most closely matched SSMI, which was persistently negative in the mid-summer. In addition, the rapid degradation in both years (mid July 2016 and late June 2020) were accompanied by near- or above-normal SPI, strongly positive EDDI, and minima of SSMI and LERI. Likely due to its larger land area, slopes of pastureland degradation in PA were much milder and more prolonged than those in MA. These milder slopes further weakened the value of PRCP

and E_0 EDDI in directing pasture conditions at this synoptic timescale regarding the violent oscillations of 1-week SPI and EDDI in both years.

Figure 18 shows the progression of 2-week indices and pasture conditions in PA during the droughts of 2016 and 2020. The dry and wet periods mentioned above are evident at this timescale. Similar to the results for MA, SSMI has the closest correspondence to pastureland degradation. Whenever SSMI dropped below -1.0, pasture conditions also entered a period of degradation (mid June 2016, early September 2016, early November 2016, late June 2020, mid August 2020, and late September 2020). For EDDI, dates of maximal values (EDDI greater than 1.5) match pastureland degradation (late June and late July in both years). Additionally, pasture conditions improved in both years when EDDI showed wetting signals in the fall (early October 2016 and early November 2020). However, for SPI, such correspondence was not evident: 2-week SPI in August 2016 was repeatedly above 0.8, but pasture conditions merely stopped worsening instead of improving. This can also be found for early to mid August 2020 when SPI remained above 1.0 but pasture conditions continued to degrade.

Figure 19 shows the 1-month indices and the pasture conditions in PA during the drought years of 2016 and 2020. At this timescale, all indices showed good correspondence to pastureland degradation. The periods in both years when degradation started were almost exactly when the four indices reached their first minima (maxima for EDDI), during mid to late June. EDDI and SSMI remained negative as pastureland degradation continued, so they matched more closely to pasture conditions than SPI and

SPEI did. As at the 2-week timescale, 1-month SPI and SPEI switched to positive in August of both years, but the pastureland degradation did not respond.

Figure 20 shows the 3-month indices and the pasture conditions in PA during the drought years of 2016 and 2020. Similar to MA, SSMI at this timescale does not correspond to pastureland degradation. The 3-month SSMI in 2016 remained below -0.6 and only decreased in late May when pasture conditions were improving. In 2020, pastureland degradation started when the 3-month SSMI was at its maximal (late June). 3-month EDDI in both years also demonstrated little correspondence: pasture conditions started to degrade when 3-month EDDI was near normal. For 3-month SPI and SPEI, their pattern in 2020 also showed little correspondence to the pasture conditions. However, in 2016, the below-normal SPI (and SPEI) in the summer and the above-normal SPI in October matched the pasture conditions degradation and recovery.

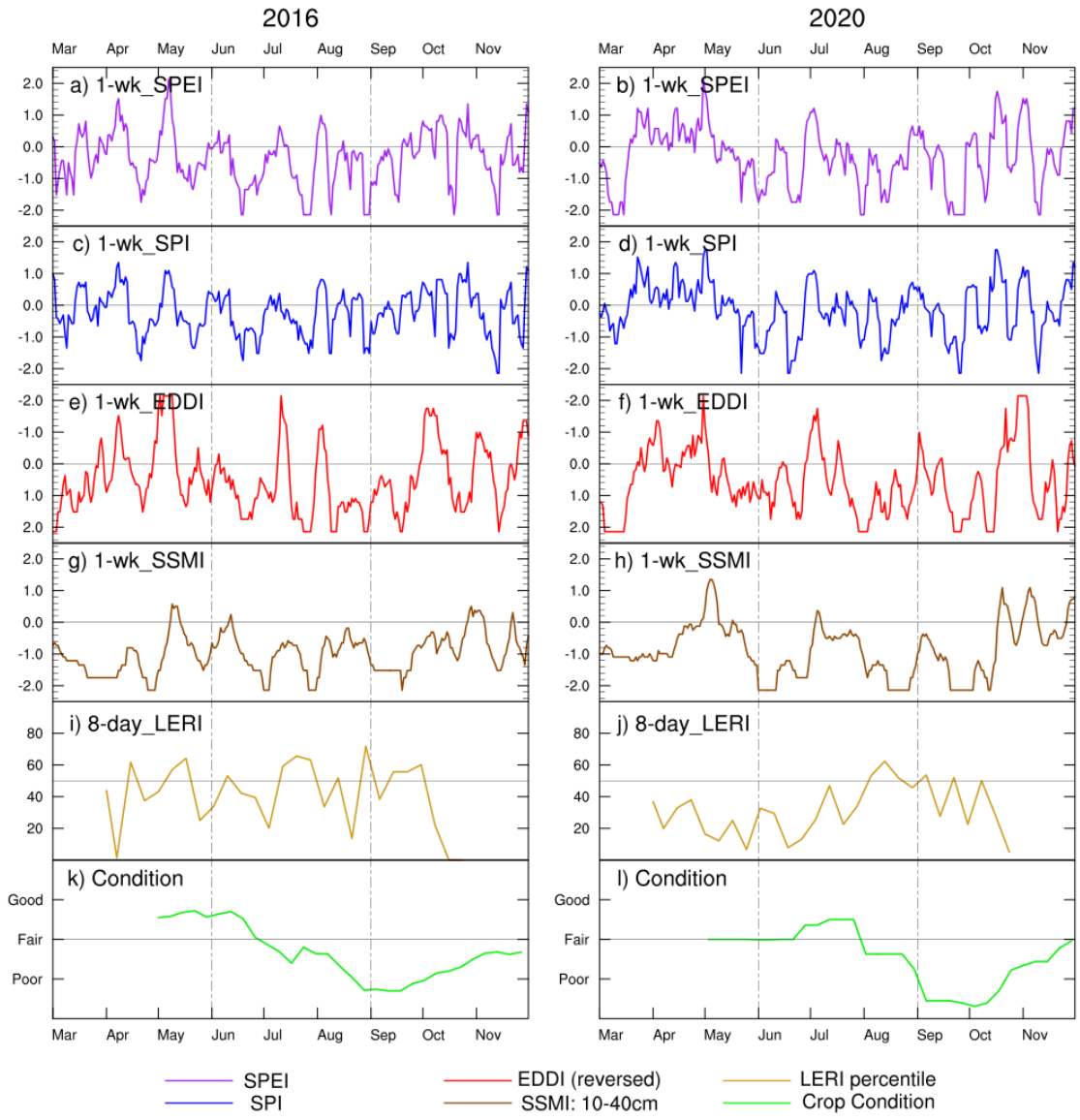

Figure 13. Time Series of 1-week drought indices (a - j) and pasture conditions (k, l) in Massachusetts from March to December in 2016 and 2020.

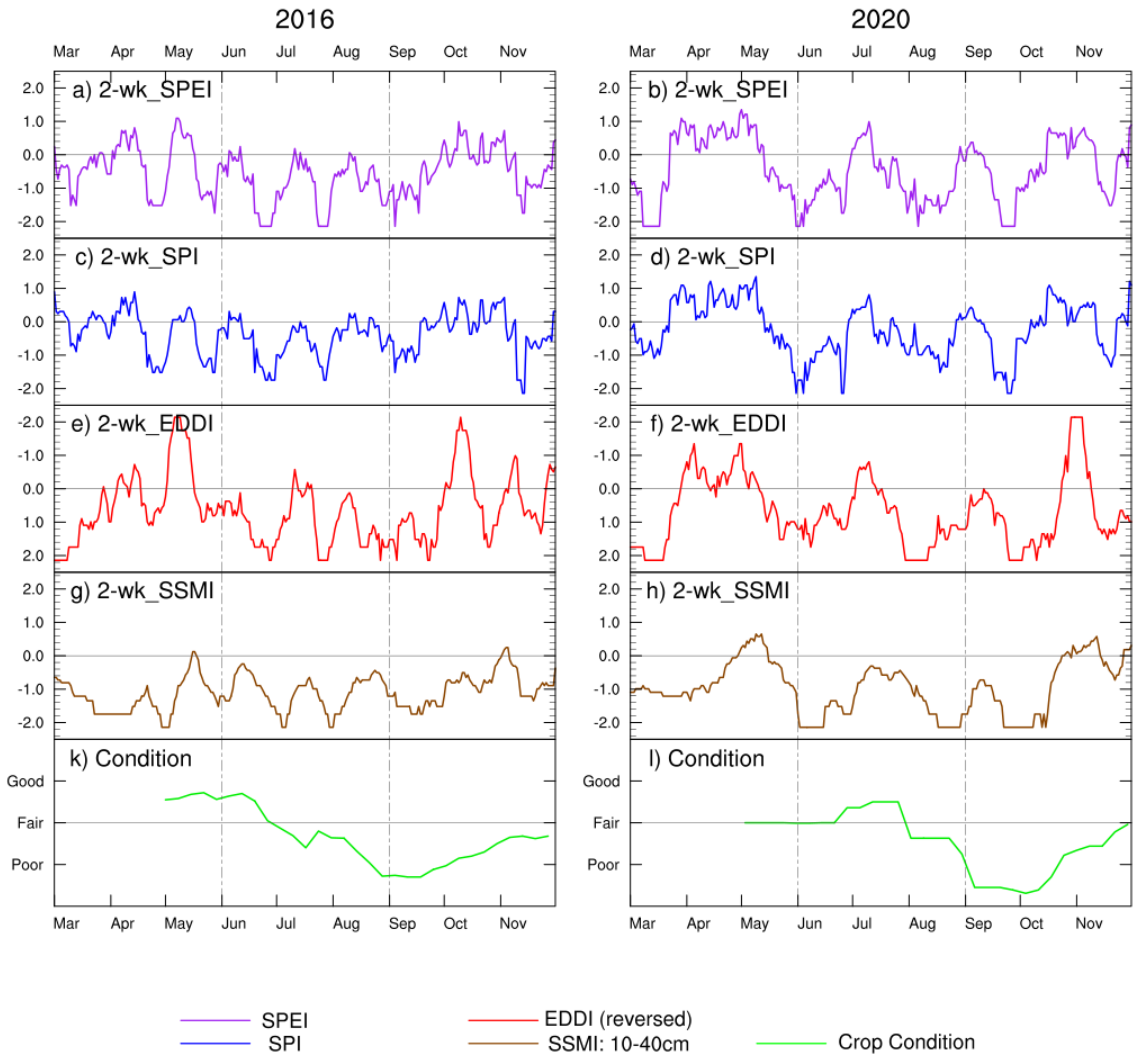

Figure 14. Time Series of 2-week drought indices (a - h) and pasture conditions (k, l) in Massachusetts from March to December in 2016 and 2020.

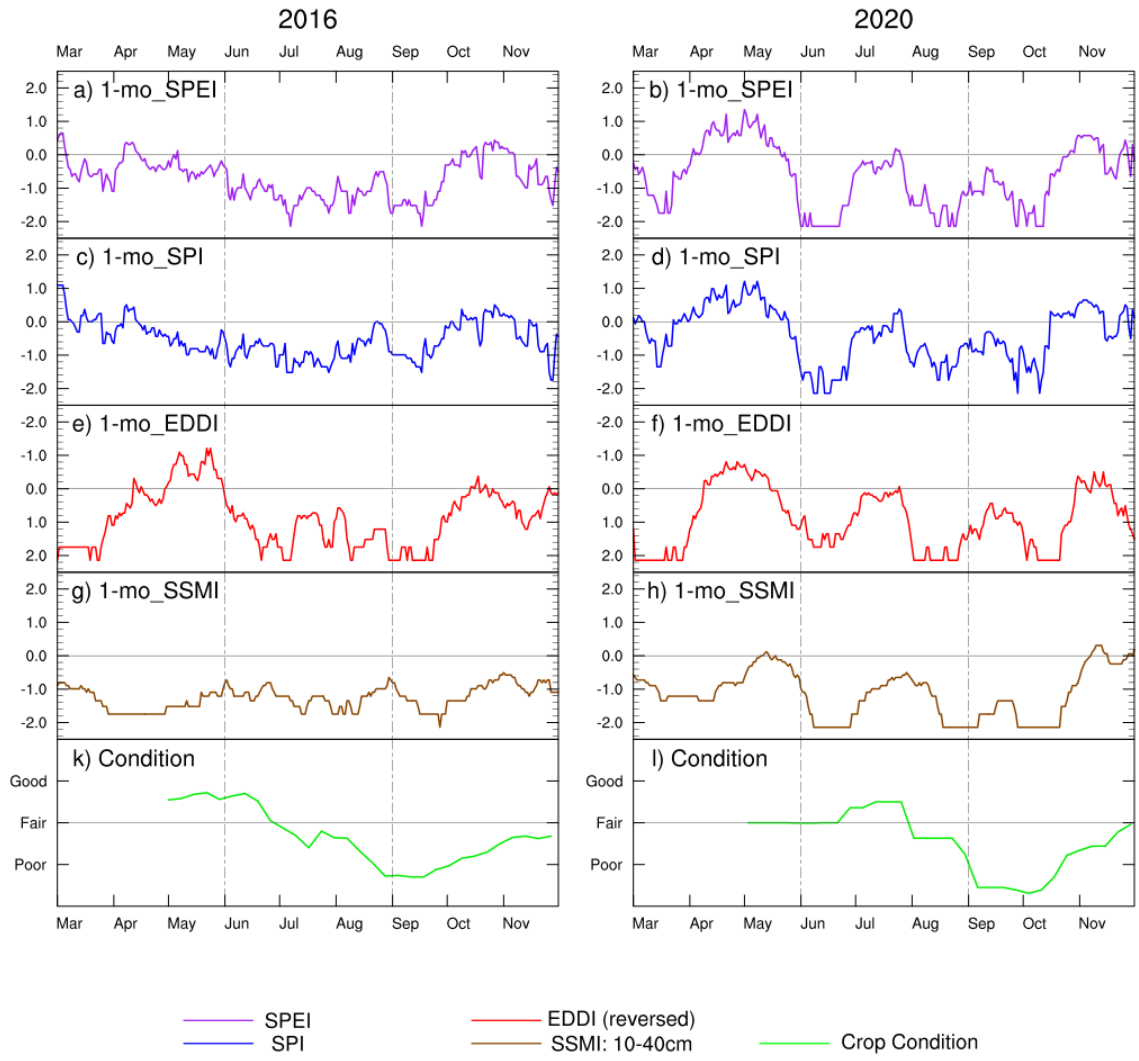

Figure 15. Time Series of 1-month drought indices (a - h) and pasture conditions (k, l) in Massachusetts from March to December in 2016 and 2020.

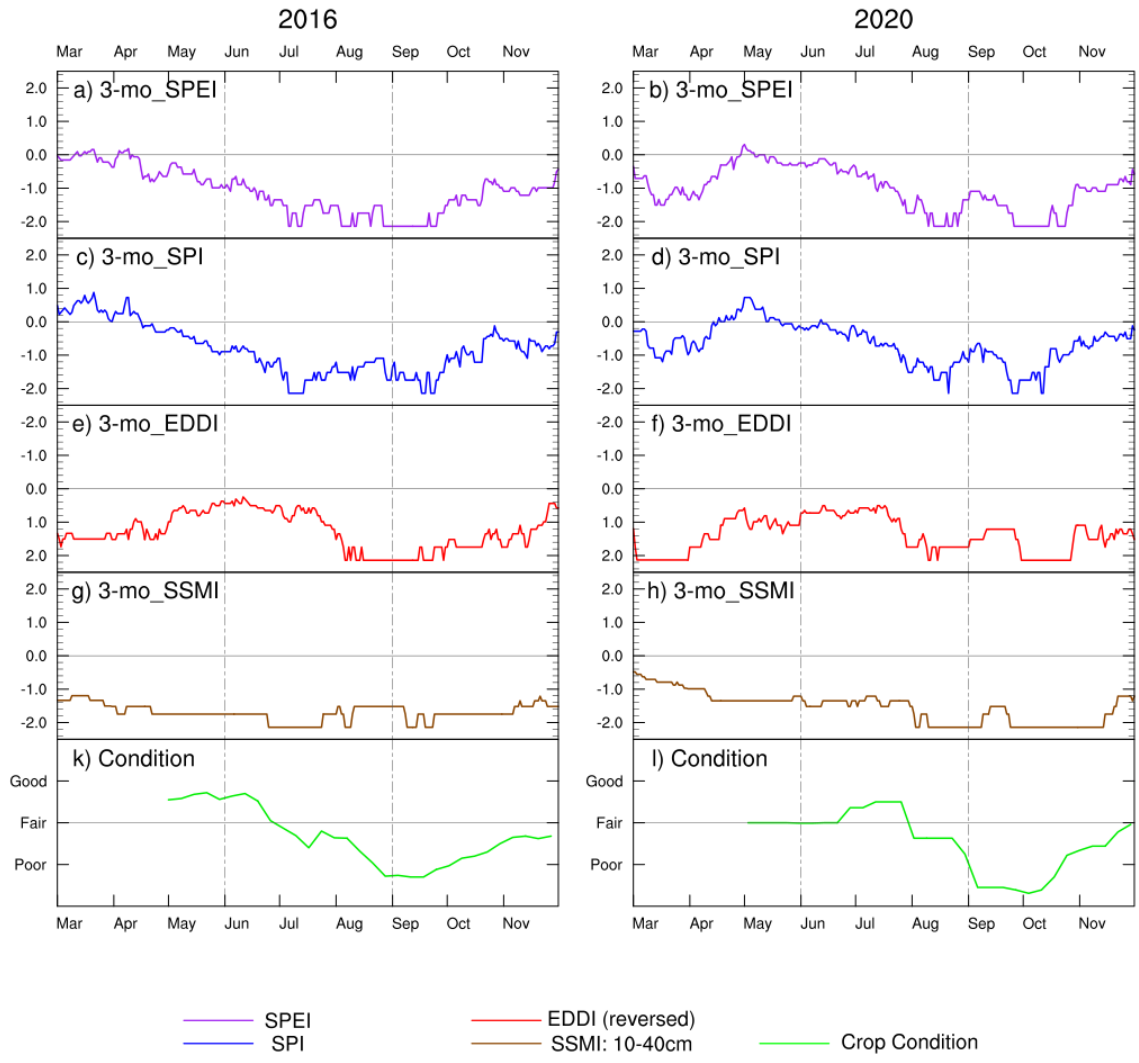

Figure 16. Time Series of 3-month drought indices (a - h) and pasture conditions (k, l) in Massachusetts from March to December in 2016 and 2020.

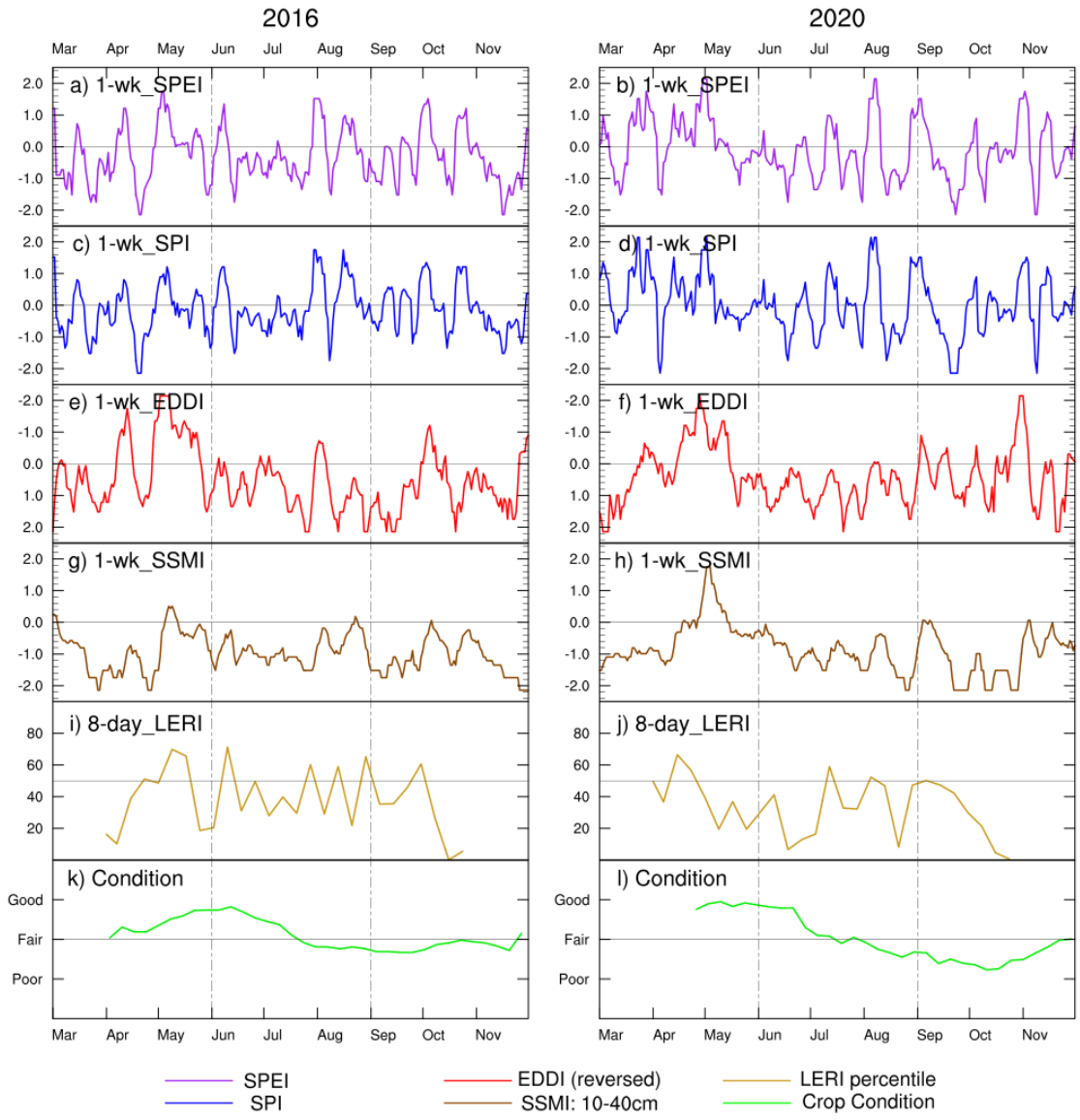

Figure 17. Time Series of 1-week drought indices (a - j) and pasture conditions (k, l) in Pennsylvania from March to December in 2016 and 2020.

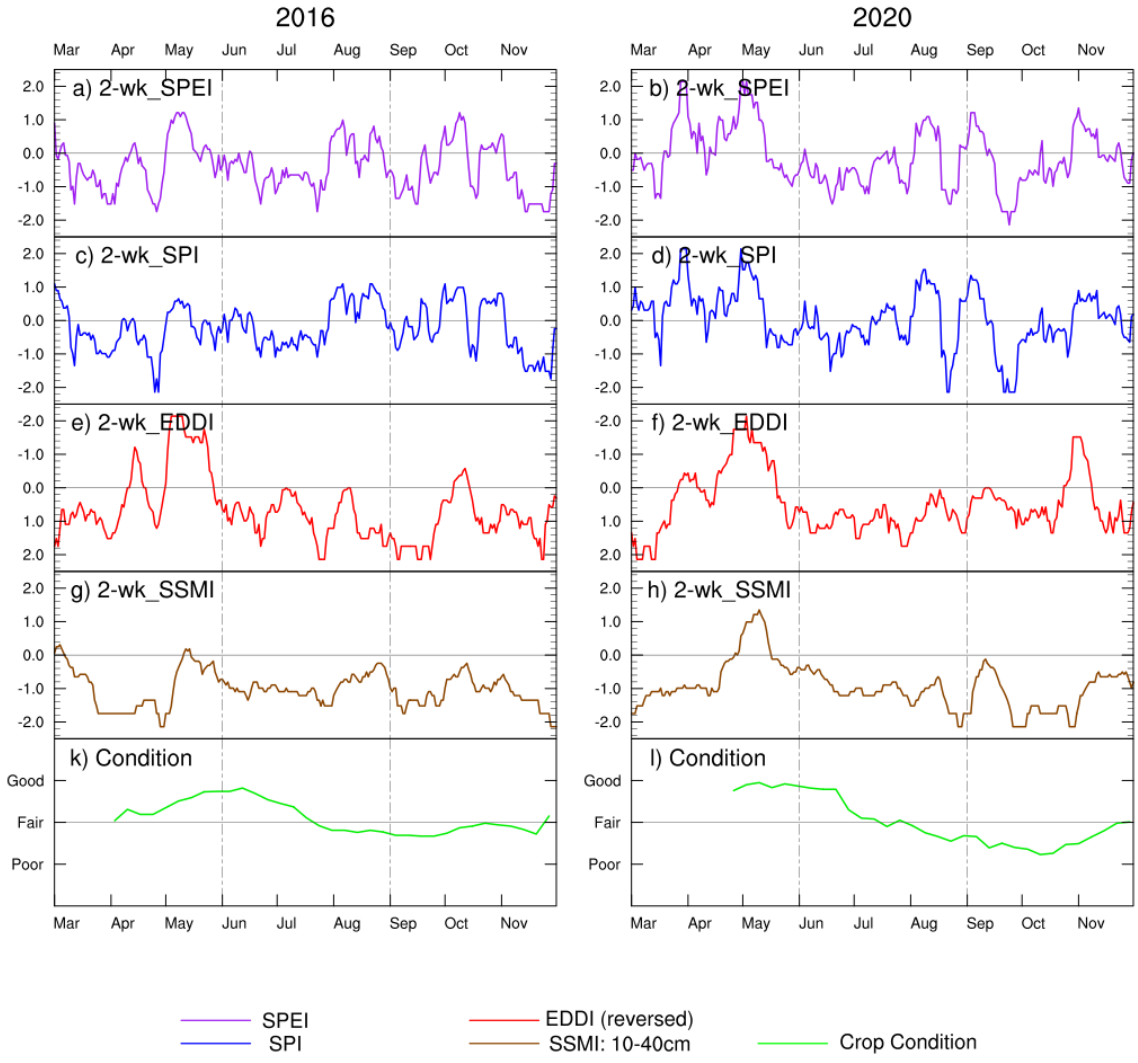

Figure 18. Time Series of 2-week drought indices (a - h) and pasture conditions (k, l) in Pennsylvania from March to December in 2016 and 2020.

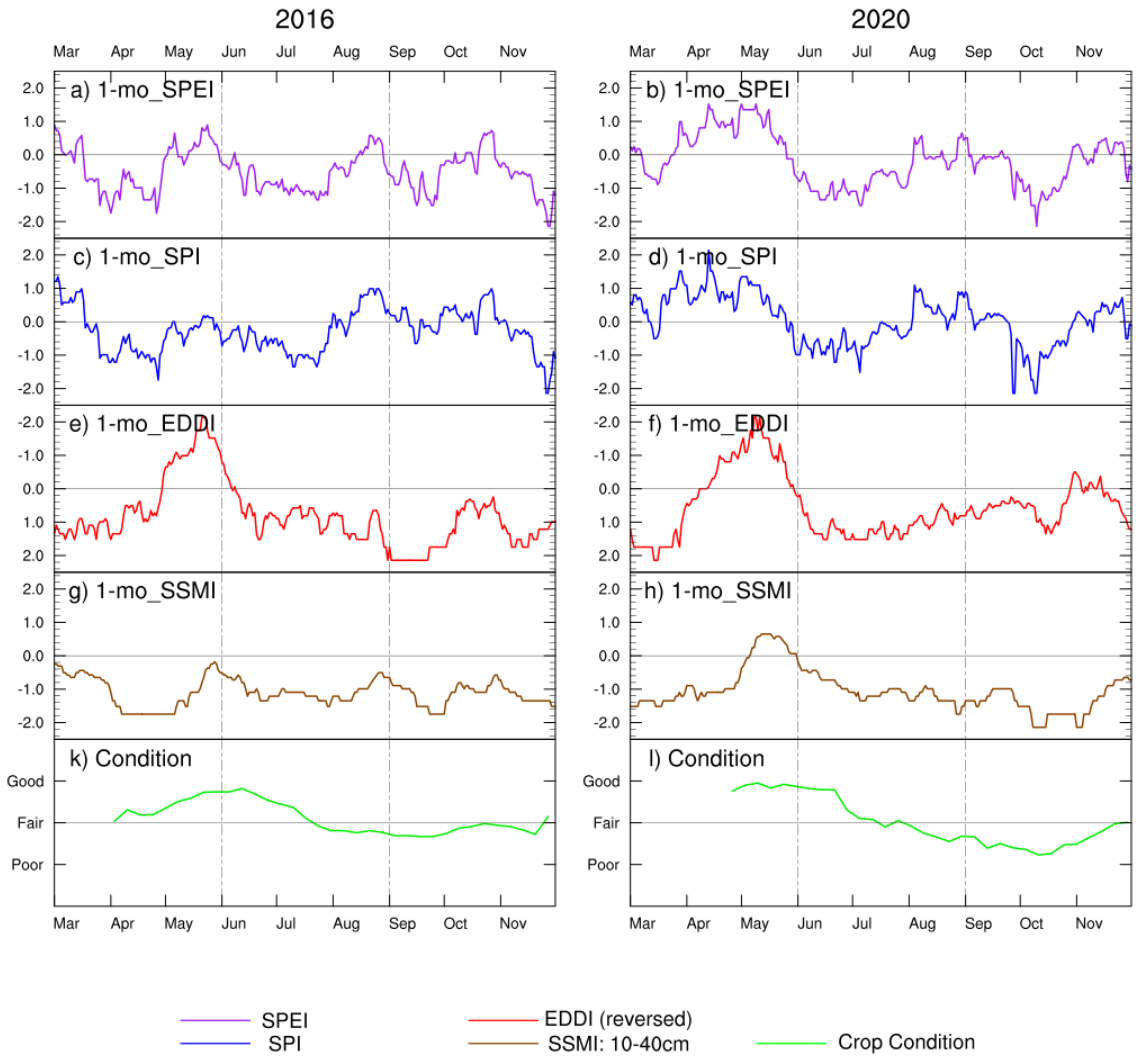

Figure 19. Time Series of 1-month drought indices (a - h) and pasture conditions (k, l) in Pennsylvania from March to December in 2016 and 2020.

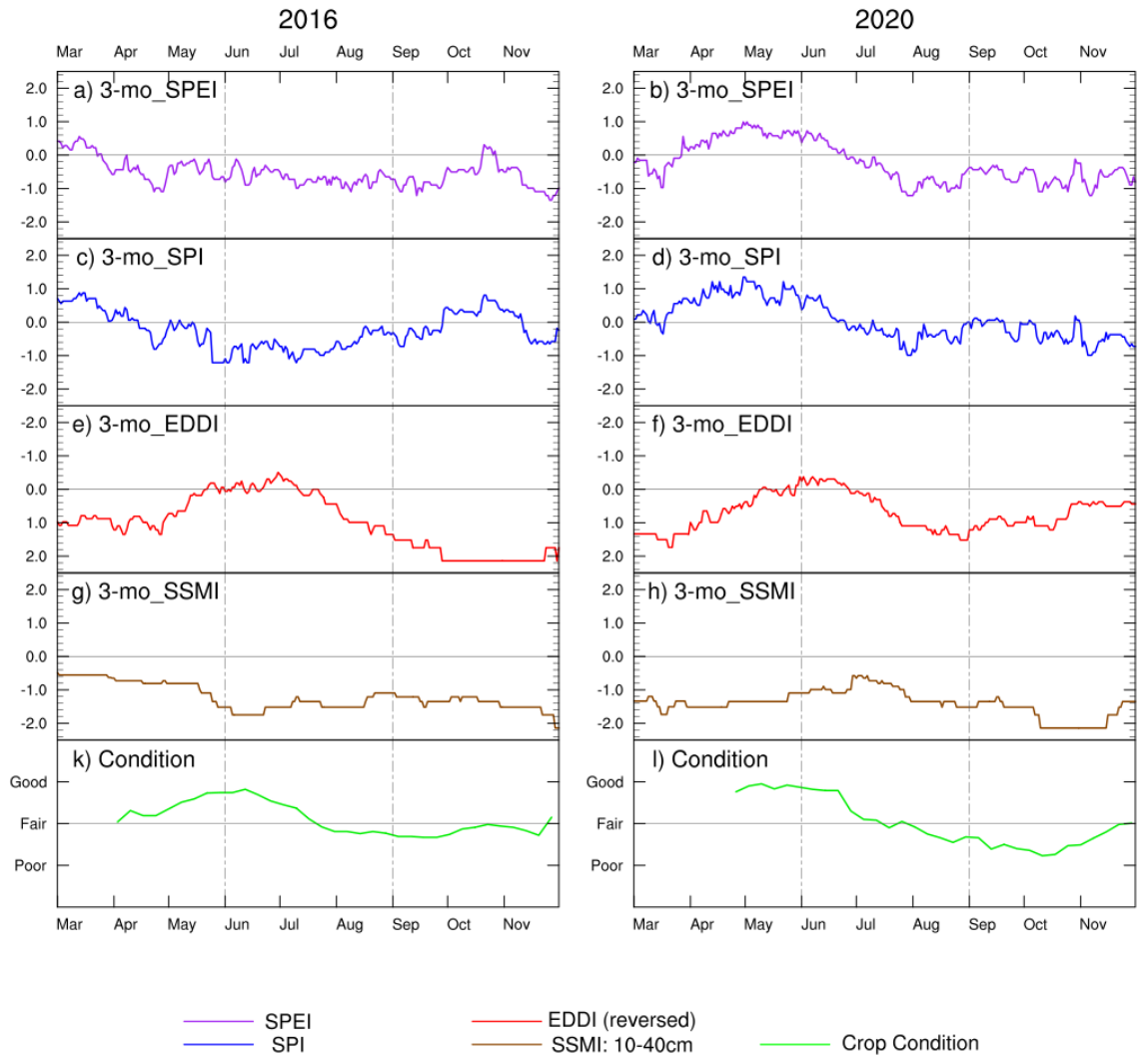

Figure 20. Time Series of 3-month drought indices (a - h) and pasture conditions (k, l) in Pennsylvania from March to December in 2016 and 2020.

4. Discussion and Conclusion

4.1. Discussion

4.1.1. Correlation analysis

This study first investigated the correlation between hay yield and different drought indices over the period of 1981-2020 in the Northeast and found significant correlations (R_{max}>0.304) over much of the region. Due to the complex factors affecting hay yield that are not climatic in nature, a value of |R| greater than 0.5 is generally considered strong correlation between drought indices and agricultural production in many regions including the Central Plains (Peña-Gallardo et al., 2019), Northwest (Wurster et al., 2020), and generally across the CONUS (Lu et al., 2020). Across most PA, NY, and NJ counties and the southern New England states, our results for hay were in line with these studies, showing the strongest |R| around 0.5 for all indices.

Large spatial variability can be found for the R_{max} and its associated drought-index timescale. In NH, ME, and several upper NY counties, the R_{max} for all indices were either notably weaker than in other areas or insignificant. This is likely due to the uneven distribution of planting area within the states (Figure 4) and the different hydrologic conditions around the mountainous areas (Engman, 1981). Mountain snowmelt plays a significant role in water supplies in many regions (Qin et al., 2020; Stewart, 2009). Although the water cycle in the humid Northeast is driven by year-round PRCP with no distinct dry season, areas next to a watershed where surface water comes mostly from

mountains may still receive more influence from snowmelt, usually manifested as downstream processes (e.g., groundwater recharge and ecosystem feedbacks). For a county near mountains, hay yields may be subject to local summer PRCP and the snowmelt originating from nonlocal winter PRCP in the mountains, with the ratio of local to nonlocal PRCP remaining elusive. Since all correlation coefficients in this study were obtained by comparing local data only (e.g., SPI is based on PRCP filtered by local rainfed crop coverage), signals of the connection between hay yield and nonlocal snowmelt runoff were inevitably ignored. This potentially explains why counties (and states) surrounding mountainous areas and their main watersheds (e.g., Adirondack Mountains and the Hudson River) showed weaker R for all indices (Figure 6).

The ending month of the strongest hay yield-drought index relationships also exhibited significant spatial variability. Though diverse, the combination of timescales and ending months across the Northeast were limited to four types: 1 week to 1 month ending in spring; 2 weeks to 3 months ending in summer; 3 to 6 months ending in fall; and 1 to 9 months ending in the preceding winter (Figures 7 to 8 and Table 1). Although these combinations generally pointed to the late spring and late summer (except the winter type) as displaying strong correlations, it is possible that factors not considered in this study (e.g., soil properties, groundwater levels, cultivation strategies) played roles in determining the timescales associated with the R_{max}. Similar to the findings of previous studies on other crops (Lorenzo-Lacruz et al., 2010; Pasho et al., 2011; Vicente-Serrano et al., 2013; Wurster et al., 2020), we see that these factors may alter the resilience of hay

yield against water deficit (or surplus) either by compensating for the SM anomaly or directing the physiological adaptations of hay.

This study used SPI and EDDI separately to investigate the individual effects of PRCP and E_0 on hay yield across the Northeast. Both climate drivers were shown to be closely related to hay yield but with the R being opposite in sign, with the R_{max} of EDDI being negative while that of SPI was positive in most regions (high E_0 leads to low yield and high PRCP leads to high yield). Such patterns revealed that hay yield in the region is more constrained by drying processes and extremes like drought than of wetting and flood. Many previous studies have been focused on PRCP using SPI and SPEI to characterize their sensitivity regarding crop yield (Peña-Gallardo et al., 2019; Wang et al., 2014; Zipper et al., 2016). As a drought index that simultaneously incorporates the variation in PRCP and E_0, SPEI has been found to be more representative than other indices in connecting crop production with the climate drivers (Beguería et al., 2014; Peña-Gallardo et al., 2018; Vicente-Serrano et al., 2012). However, this study found that, across the Northeast, the correlation between hay yield and SPEI was similar to that of SPI. This is most likely because PRCP greatly exceeds E_0 in the humid hydroclimate of the Northeast (annual average PRCP being 46 inches while E_0 being 25 inches; (NRCC, 2011)), which leads to anomalies in absolute values of PRCP being much more significant than those of E_0. In the development of SPEI, the input variable is the difference of PRCP minus E_0 (Vicente-Serrano et al., 2010). Therefore, regarding long-term time series in the Northeast (forty years in this study), the signal of variations in PRCP in determining SPEI are much greater than those in E_0, leading to the similarity in

R_{max} between SPEI and SPI. However, the influence of E_0 on the hay yield was evident as EDDI showed R at a similar magnitude to SPI. The only difference being that the R_{max} for SPI tended to have longer timescales than EDDI. These results highlighted the value of EDDI in impacting hay yield during dry periods when PRCP is low.

We also examined the full distribution of R at each timescale and ending month across the Northeast. The R shown for all indices at the 1- to 3-month timescales ending in the late summer are generally strong (again, R for EDDI is negative while others are positive). The response of hay yield to dry anomalies within such a time window is related to the changes in SM, which can be driven by the balance of PRCP and E_0 during summer (Hunt et al., 2014). If this seasonality coincides in time with the key phenological stages of crops, the response of yield to drought is higher (Araujo et al., 2016; Zipper et al., 2016). Hay yields in PA and MA appeared to conform to this pattern with key phenological stages centered around the late summer. Besides, the 1-week to 1-month timescales ending in late spring and 6 to 9-month ending in late fall also have considerable values of R for all indices. These high-value areas of R outlined an overall right-tilting (i.e., short timescales ending earlier and long timescales ending later in the year) trend in the distribution graph, highlighting the hay yield responding positively to PRCP and SM while negatively to E_0 throughout the growing season. It can be presumed that, for different areas in the Northeast, R within different time windows were higher than in summer due to the diverse hydrological conditions and planting strategies. This may also explain the spatial variability of the combination types (timescales and ending month) associated with the R_{max}. In addition to the overall trend, the timescales associated

with high values of R were found to be shorter for EDDI and SSMI than for SPI and SPEI. This is in line with other studies that found that crop production tends to respond to PRCP at longer timescales but to E_0 and SM at shorter timescales (Hunt et al., 2014; Wurster et al., 2020; Yamoah et al., 2000). Despite the signals indicating drought, some opposite R indicating water surplus can also be found with smaller magnitudes than drought signals. Other studies have attributed the response of crop yield to positive E_0 and negative PRCP anomalies across the CONUS to poor soil drainage (Lobell & Asner, 2003; Wurster et al., 2020; Zipper et al., 2016). In the case of the Northeast, this issue is of particular interest as flooding is also common in the region. The opposite response to drought indices (wetting as opposed to drying) was evident in areas where the flooding in late spring could be disastrous to the hay yield. For example, several adjacent counties in western NY showed positive R_{max} for EDDI at the 1- to 2-week timescale ending in spring, indicating that increased E_0 could alleviate the waterlogging during the period and thus increase the hay yield.

We also examined the correlations between hay yield and SM at different depths across the Northeast. Similar to the results for other indices, the overall R for all three layers of SSMI were strong (strongest $|R| > 0.5$) except for those counties and states neighboring mountainous regions. The temporal distribution of R in PA and MA for all SSMI showed a similar pattern to that of EDDI (with opposite signs) and was centered around 1-week to 3-month timescales ending in the summer. Such timescales are generally shorter than those for SPI and SPEI. As an essential water availability factor for crop development during the key phenological stages (Barnabás et al., 2008; Ramadas &

Govindaraju, 2015), SM anomalies impose almost immediate and direct physiological impacts on crops. So does E_0, which can rapidly deplete SM during heat waves (Beguería et al., 2014). However, insufficient PRCP must persist for some time before it is reflected in reduced SM to affect crop development. Therefore, compared to EDDI and SSMI, SPI has relatively longer timescales when associated with hay yield. In addition, for SSMI at different depths, the R_{max} between surface SSMI and hay yield was significantly greater than that of deeper SSMI. This is in line with the effective rootzone depth for hay which is from 0 to 40 cm (Efetha et al., 2009; Irmak et al., 2007), corresponding to the 0-10 cm and 10-40 cm levels we examined. This pattern was also confirmed by the temporal distribution of R in PA and MA, which was similar for all depths, with stronger R in the shallow layers.

4.1.2. Time Series comparison

In most New England states, pasture conditions during the droughts of 2016 and 2020 were the worst in the last 25 years. Conditions in both years began as average in the spring, but experienced severe declines in the summer. This decline was also seen in PA. It corresponds well in time with the drought in the Northeast in both years indicated by USDM. This study selected MA and PA to compare the progression of pasture conditions in 2016 and 2020 with the contemporaneous time series of drought indices. Different timescales of drought indices were examined to identify the time required for drought signals in each climate driver to accumulate to impact pasture conditions.

Comparison to the SSMI showed that pasture conditions were most responsive to the short-range SM anomalies (1- to 2-week timescales in MA and 1-week to 1-month timescales in PA), the component directly related to the plant water use. Within these timescales, the pasture conditions correspond closely to the fluctuation of SSMI. It is worth noting that SSMI at these timescales was above normal in late spring in both years, which can be corroborated by the improvement of condition during the same time. This indicates that the impact of drought on pasture in these two years was limited to summer and fall. The above-normal SSMI was unavailable at longer timescales, by which SSMI was consistently below normal due to the drying anomalies throughout the year. When comparing SSMI to SPI and EDDI at these short timescales, we identified a clear response of SSMI to both, which is most likely due to the forcing of PRCP and E_0 at synoptic scales. This response has a time lag such that variation in SSMI is around one week behind that in SPI and EDDI. This time lag effect is common between SM and meteorological forcings due to the memory of soil (Koster & Suarez, 2001; W. Wu & Dickinson, 2004). It lengthens the response time of pasture conditions to short-term anomalies in SPI and EDDI.

At the 1-week to 1-month timescales in PA and MA, SPI and EDDI showed mostly opposite trends in 2016 and 2020. This is expected, as wet weather (high PRCP) is often simultaneously associated with low E_0 (vice versa for dry weather). However, several exceptions were also found when high EDDI was accompanied by normal or high SPI. In these cases, pasture conditions continued declining when above-normal E_0 occurred with normal PRCP but stopped declining or started improving when E_0 and

PRCP were both strong, regardless of SM anomalies. This could be a coincidence (two years at two states represents a small sample size) caused by the mixing of signals as pasture conditions may respond to PRCP and E_0 at different, longer timescales. If not, one assumption would be that the short-term (1- to 2-week timescale) extra PRCP during periods of high E_0 may quickly be consumed in the plant water use to improve crop conditions and thus fail to cause sufficient changes in SM. However, this assumption was rejected because the SPEI time series almost perfectly followed the SPI curve in both years and both states, which indicated that the high E_0 only offset a small fraction of the PRCP in terms of water amount. However, using EDDI alone still has value in tracking pastureland degradation during drought. Of all the indices at the timescales of 2-week to 1-month, dry signals in EDDI can be best fit to the pasture conditions. This is most likely because E_0 can directly lead to increased ET which can deplete the SM and thus introduce a more immediate physiological response on pasture conditions than PRCP (Wurster et al., 2020). SPI, on the other hand, fits best to pasture conditions at timescales of 1 to 3 months. As noted, SM during the late spring in both years was above normal. In this case, the subsequent deficit of PRCP may be offset by the residual SM excess in the early summer, which may lead to pasture conditions lagging the impact of PRCP as seen in SPI (Sánchez et al., 2016; Zhao et al., 2018). The fundamental reason for this delay is that the lack of PRCP can only indirectly reduce SM through accumulation over time and thus takes longer to force a pasture response. For timescales longer than 3 months, only the 6-month SPI of 2016 in PA showed good correspondence with pasture conditions. At such longer timescales, some indices showed temporal discrepancies relative to pastureland degradation; some were flattened to be consistently below normal throughout

the years due to the long-term dry anomalies. In general, all drought indices at timescales longer than 6 months failed to show any correspondence with pasture conditions in 2016 and 2020.

Specifically for the 1-week timescale, LERI showed dry anomaly below the 50th percentile for most of the summer for both years in MA and PA. The low LERI in the summers were in the same time windows as the pastureland degradation. This highlights the potential use of LERI in signaling the impact of drought on pasture health. With the exception of MA after August, all LERI curves correlated well with 1-week SSMI in both states and both years. In summary, every decline and increase in LERI corresponds to a simultaneous variation of SSMI. Such a degree of correspondence was seldom found when comparing LERI to SPI or EDDI. This suggests that, in 2016 and 2020, especially during the pasture's pre-fall growing season, the variation of ET was more constrained by changes in SM than in PRCP or E_0. This is in line with the moisture-limited situation in the complementary relationship (CR) between ET and E_0 (see section 2.1.1, Figure 3; (Bouchet, 1963)), as SM becomes the major factor limiting ET during sustained drought. For both states in both years, the moisture-limited situation reflected by such a SM-ET coupling was already in place before pasture degradation started. This is mostly likely due to the poor SM condition in the early springs of both years and explains why little synchronous variation of LERI and EDDI was found (year-long moisture-limited for both). In drought, even humid areas like the Northeast can have periods of water limitation and thus act like arid areas. The validity and applicability of the CR have been tested for the arid and semi-arid areas across the US (M. T. Hobbins et al., 2001, 2004;

Huntington et al., 2011). The CR is also one of the key land-atmosphere interactions that formed the physical basis for EDDI (M. T. Hobbins et al., 2016). This functionality of EDDI was further confirmed in terms of drought impacts on crop conditions by our results. In both years and both states, several periods with SPI showing normal or wet signals were accompanied by positive EDDI (e.g., early July and mid August 2016 in MA, late July 2016 and late June 2020 in PA). LERI and SSMI during these periods either showed below normal or minimum values. Given that SPI and EDDI at the 1-week timescale almost always showed a similar wet/dry signal, the positive EDDI is most likely due to the mechanism suggested by CR. In moisture-limited situations, the energy that would have been used for ET was released from the surface as sensible heat. This interacts with the depressed vapor pressure caused by the lack of ET leading to elevated E_0. It is worth noting that these periods coincide with the most severe stages of pastureland degradation. We speculate that the pre-existing SM deficit only provided the premise of inadequate water supply, while it was this ET-E_0 dynamic that triggered the degradation process. Given the resilience of different crop types against drought (apparently low for pasture), this finding would shed light on when to expect a decline in crop conditions under sustained SM deficit or pre-existing drought.

4.2. Conclusion

Based on this study we can conclude the following:

i) Clear, strong connections were identified between the multi-decadal crop yield record and the drought indices representing PRCP, E_0, and SM in most areas of the Northeast.

ii) Among the strongest connections are signals indicating more PRCP brings more yield while higher E_0 causes less yield (and vice versa). This indicates that drought forcing is still the primary climatic factor affecting crop yields in the Northeast, especially during summer and fall despite the humid nature of the region.

iii) These connections showed substantial spatial and temporal variability in the Northeast. For example, crop yield tends to have a weaker response to the local hydroclimatic driving fluxes (PRCP, E0, and ET) and state (SM) in areas near mountain drainages. The impact of wet anomalies (e.g., excess PRCP and low E_0) in the springs was also shown by drought indices. Though less than for drought, these wet anomalies hindered crop yield, too.

iv) Different climate drivers affect crop conditions at different timescales. 2016 and 2020 were the worst two years for crop conditions on record in most Northeastern states. In both years, the drought-driven pastureland degradation was best attributed to, respectively, one to two weeks of SM deficit, two weeks to one month of elevated E_0, and one to three months of PRCP deficit. All these timescales outlined a critical period for pasture regarding drought, which is about one to two months starting from early summer. The exact numbers vary for different crop types with different resilience (e.g., hay yield responded to two weeks to three months of elevated E_0, and three to six months of PRCP deficit). One thing in common is that, when impacting crop conditions during drought, the timescales of E_0 always appeared shorter than that of PRCP. Such distinctions highlighted the necessity and importance of using multiple indices and timescales for drought monitoring.

v) As a drought index that was repeatedly proven to correlate better with vegetation production than SPI, SPEI showed highly similar results to SPI in this study. This is mostly due to the humid hydroclimate of the Northeast where the magnitudes of PRCP anomalies tend to dominate E_0 anomalies.

vi) In 2016 and 2020, the variation of ET matched most closely to that of SM, suggesting moisture-limited situations throughout both years. In the presence of SM deficits, the lack of ET was usually accompanied by enhanced E_0 in both years, regardless of PRCP. Their co-occurrence suggests that this interaction most likely triggered the degradation of pastureland during the drought.

5. Bibliography

Abatzoglou, J. T. (2013). Development of gridded surface meteorological data for ecological applications and modelling. *International Journal of Climatology*, *33*(1), 121–131. https://doi.org/10.1002/joc.3413

Abramowitz, M., & Stegun, I. A. (1964). *Handbook of mathematical functions with formulas, graphs, and mathematical tables* (Vol. 55). US Government printing office.

AghaKouchak, A., Cheng, L., Mazdiyasni, O., & Farahmand, A. (2014). Global warming and changes in risk of concurrent climate extremes: Insights from the 2014 California drought. *Geophysical Research Letters*, *41*(24), 8847–8852.

Alessi, M. J., Herrera, D. A., Evans, C. P., DeGaetano, A. T., & Ault, T. R. (2022). Soil Moisture Conditions Determine Land-Atmosphere Coupling and Drought Risk in the Northeastern United States. *Journal of Geophysical Research: Atmospheres*, e2021JD034740.

Allen, R. G., Pereira, L. S., Raes, D., & Smith, M. (1998). Crop evapotranspiration-Guidelines for computing crop water requirements-FAO Irrigation and drainage paper 56. *Fao*, *Rome*, *300*(9), D05109.

Araujo, J. A., Abiodun, B. J., & Crespo, O. (2016). Impacts of drought on grape yields in Western Cape, South Africa. *Theoretical and Applied Climatology*, *123*(1), 117–130.

Ash, A., McIntosh, P., Cullen, B., Carberry, P., & Smith, M. S. (2007). Constraints and opportunities in applying seasonal climate forecasts in agriculture. *Australian*

Journal of Agricultural Research, *58*(10), 952–965.

Barksdale, H. C. (1968). *The northeast water supply crisis of the 1960's*. US Government Printing Office.

Barlow, M., Nigam, S., & Berbery, E. H. (2001). ENSO, Pacific decadal variability, and U.S. summertime precipitation, drought, and stream flow. *Journal of Climate*, *14*(9), 2105–2128. https://doi.org/10.1175/1520-0442(2001)014<2105:EPDVAU>2.0.CO;2

Barnabás, B., Jäger, K., & Fehér, A. (2008). The effect of drought and heat stress on reproductive processes in cereals. *Plant, Cell & Environment*, *31*(1), 11–38.

Beguería, S., Vicente-Serrano, S. M., Reig, F., & Latorre, B. (2014). Standardized precipitation evapotranspiration index (SPEI) revisited: parameter fitting, evapotranspiration models, tools, datasets and drought monitoring. *International Journal of Climatology*, *34*(10), 3001–3023.

Bigelow, D. P., & Borchers, A. (2017). Major uses of land in the United States, 2012. *Economic Information Bulletin*, *178*, 1–62. www.ers.usda.gov

Blum, A. (1996). Crop responses to drought and the interpretation of adaptation. In *Drought tolerance in higher plants: Genetical, physiological and molecular biological analysis* (pp. 57–70). Springer.

Bolten, J. D., Crow, W. T., Zhan, X., Jackson, T. J., & Reynolds, C. A. (2009). Evaluating the utility of remotely sensed soil moisture retrievals for operational agricultural drought monitoring. *IEEE Journal of Selected Topics in Applied Earth Observations and Remote Sensing*, *3*(1), 57–66.

Bouchet, R. J. (1963). Évapotranspiration Réelle Et Potentielle Signification Climatique.

International Association of Science and Hydrology, *62*, 134–162. https://iahs.info/uploads/dms/iahs_062_0134.pdf%0Ahttp://hydrologie.org/redbooks/a062/iahs_062_0134.pdf

Bush, T., Ogle, D., John, L. S., Stannard, M., & Jensen, K. (2012). *Plant guide for orchardgrass (Dactylis glomerata).* Aberdeen Plant Materials Center, Aberbeen, ID.

Cai, X., Yang, Z., Xia, Y., Huang, M., Wei, H., Leung, L. R., & Ek, M. B. (2014). Assessment of simulated water balance from Noah, Noah-MP, CLM, and VIC over CONUS using the NLDAS test bed. *Journal of Geophysical Research: Atmospheres*, *119*(24), 13–751.

Carrão, H., Russo, S., Sepulcre-Canto, G., & Barbosa, P. (2016). An empirical standardized soil moisture index for agricultural drought assessment from remotely sensed data. *International Journal of Applied Earth Observation and Geoinformation*, *48*, 74–84. https://doi.org/10.1016/j.jag.2015.06.011

Collins, K., Hannaford, J., Svoboda, M., Knutson, C., Wall, N., Bernadt, T., Crossman, N., Overton, I., Acreman, M., & Bachmair, S. (2016). Stakeholder coinquiries on drought impacts, monitoring, and early warning systems. *Bulletin of the American Meteorological Society*, *97*(11), ES217–ES220.

CPC. (2021). *US Drought Information - NOAA NWS*. https://www.cpc.ncep.noaa.gov/products/Drought/

Crausbay, S. D., Ramirez, A. R., Carter, S. L., Cross, M. S., Hall, K. R., Bathke, D. J., Betancourt, J. L., Colt, S., Cravens, A. E., & Dalton, M. S. (2017). Defining ecological drought for the twenty-first century. *Bulletin of the American Meteorological Society*, *98*(12), 2543–2550.

Dai, A. (2011). Drought under global warming: a review. *Wiley Interdisciplinary Reviews: Climate Change*, *2*(1), 45–65.

Dai, A., Zhao, T., & Chen, J. (2018). Climate change and drought: a precipitation and evaporation perspective. *Current Climate Change Reports*, *4*(3), 301–312.

Daly, C., Neilson, R. P., & Phillips, D. L. (1994). A statistical-topographic model for mapping climatological precipitation over mountainous terrain. *Journal of Applied Meteorology and Climatology*, *33*(2), 140–158.

Degaetano, A. T. (1999). A temporal comparison of drought impacts and responses in the New York City metropolitan area. *Climatic Change*, *42*(3), 539–560. https://doi.org/10.1023/A:1005413410160

Dieter, C. A. (2018). *Water availability and use science program: Estimated use of water in the United States in 2015*. Geological Survey.

Dupigny-Giroux, L.-A., Mecray, E., Lemcke-Stampone, M., Hodgkins, G. A., Lentz, E. E., Mills, K. E., Lane, E. D., Miller, R., Hollinger, D., Solecki, W. D., Wellenius, G. A., Sheffield, P. E., MacDonald, A. B., & Caldwell, C. (2018). *Chapter 18 : Northeast. Impacts, Risks, and Adaptation in the United States: The Fourth National Climate Assessment, Volume II*. US Global Change Research Program. https://doi.org/10.7930/NCA4.2018.CH18

Efetha, A., Dow, T., McKenzie, R. H., Bennett, D. R., & Hohm, R. A. (2009). Effect of irrigation management on yield and water use efficiency of timothy hay in southern Alberta. *Canadian Journal of Plant Science*, *89*(6), 1075–1088.

Engman, E. T. (1981). Rainfall-runoff characteristics for a mountainous watershed in the Northeast United states. *Hydrology Research*, *12*(4–5), 247–264.

Erdman, J. (2020). *New England Drought Has Reached Extreme Levels With Record Dry September, But Rain Is Back, At Last*. The Weather Channel. https://weather.com/forecast/regional/news/2020-09-25-new-england-drought-relief-ahead-forecast

Evans, P. S. (1978). Plant root distribution and water use patterns of some pasture and crop species. *New Zealand Journal of Agricultural Research, 21*(2), 261–265.

Farahmand, A., & AghaKouchak, A. (2015). A generalized framework for deriving nonparametric standardized drought indicators. *Advances in Water Resources, 76,* 140–145.

Fernando, D. N., Mo, K. C., Fu, R., Pu, B., Bowerman, A., Scanlon, B. R., Solis, R. S., Yin, L., Mace, R. E., & Mioduszewski, J. R. (2016). What caused the spring intensification and winter demise of the 2011 drought over Texas? *Climate Dynamics*, *47*(9), 3077–3090.

Frumhoff, P. C., McCarthy, J. J., Melillo, J. M., Moser, S. C., & Wuebbles, D. J. (2007). Confronting Climate Change in the U.S. Northeast: Science, Impacts, and Solutions. Synthesis report of the Northeast Climate Impacts Assessment (NECIA). *Strategies,* 160.

Frumhoff, P. C., McCarthy, J. J., Melillo, J. M., Moser, S. C., Wuebbles, D. J., Wake, C., & Spanger-Siegfried, E. (2008). An integrated climate change assessment for the Northeast United States. *Mitigation and Adaptation Strategies for Global Change*, *13*(5), 419–423.

Giannini, A., Saravanan, R., & Chang, P. (2003). Oceanic forcing of Sahel rainfall on interannual to interdecadal time scales. *Science*, *302*(5647), 1027–1030.

Giorgi, F., Im, E. S., Coppola, E., Diffenbaugh, N. S., Gao, X. J., Mariotti, L., & Shi, Y. (2011). Higher hydroclimatic intensity with global warming. *Journal of Climate*, *24*(20), 5309–5324. https://doi.org/10.1175/2011JCLI3979.1

Goslee, S., & Gonet, J. (2018). *Pasture Plants of the Northeastern US* (Issue March). http://grazingguide.net/pdfs/plantguide/PasturePlantGuide-2018_01Introduction.pdf

Grigg, N. S. (2014). The 2011–2012 drought in the United States: new lessons from a record event. *International Journal of Water Resources Development*, *30*(2), 183–199.

Hayes, M., Svoboda, M., Wall, N., & Widhalm, M. (2011). The lincoln declaration on drought indices: Universal meteorological drought index recommended. *Bulletin of the American Meteorological Society*, *92*(4), 485–488. https://doi.org/10.1175/2010BAMS3103.1

Hayhoe, K., Wake, C. P., Huntington, T. G., Luo, L., Schwartz, M. D., Sheffield, J., Wood, E., Anderson, B., Bradbury, J., & DeGaetano, A. (2007). Past and future changes in climate and hydrological indicators in the US Northeast. *Climate Dynamics*, *28*(4), 381–407.

Henderson, J., & Kauffman, N. (2012). Initial Impacts of the 2012 Drought. In *The Main Street Economist* (Issue 3). http://www.kansascityfed.org/publicat/mse/MSE_0312.pdf

Hobbins, M., Mcevoy, D., & Hain, C. (2017). Evapotranspiration, Evaporative Demand, and Drought. In *Drought and Water Crisis* (1st ed., pp. 259–288).

Hobbins, M. T., Ramírez, J. A., & Brown, T. C. (2004). Trends in pan evaporation and actual evapotranspiration across the conterminous U.S.: Paradoxical or

complementary? *Geophysical Research Letters*, *31*(13). https://doi.org/10.1029/2004GL019846

Hobbins, M. T., Ramírez, J. A., Brown, T. C., & Claessens, L. H. J. M. (2001). The complementary relationship in estimation of regional evapotranspiration: The Complementary Relationship Areal Evapotranspiration and Advection-Aridity models. *Water Resources Research*, *37*(5), 1367–1387. https://doi.org/10.1029/2000WR900358

Hobbins, M. T., Wood, A., McEvoy, D. J., Huntington, J. L., Morton, C., Anderson, M., & Hain, C. (2016). The Evaporative Demand Drought Index. Part I: Linking Drought Evolution to Variations in Evaporative Demand. *Journal of Hydrometeorology*, *17*(6), 1745–1761. https://doi.org/10.1175/JHM-D-15-0121.1

Hoerling, M., Eischeid, J., Kumar, A., Leung, R., Mariotti, A., Mo, K., Schubert, S., & Seager, R. (2014). Causes and predictability of the 2012 great plains drought. *Bulletin of the American Meteorological Society*, *95*(2), 269–282. https://doi.org/10.1175/BAMS-D-13-00055.1

Howitt, R., Medellín-Azuara, J., MacEwan, D., Lund, J. R., & Sumner, D. (2015). *Economic analysis of the 2015 drought for California agriculture*. Center for Watershed Sciences University of California, Davis, CA.

Huang, J., Yu, H., Guan, X., Wang, G., & Guo, R. (2016). Accelerated dryland expansion under climate change. *Nature Climate Change*, *6*(2), 166–171.

Hunt, E. D., Svoboda, M., Wardlow, B., Hubbard, K., Hayes, M., & Arkebauer, T. (2014). Monitoring the effects of rapid onset of drought on non-irrigated maize with agronomic data and climate-based drought indices. *Agricultural and Forest*

Meteorology, *191*, 1–11. https://doi.org/10.1016/j.agrformet.2014.02.001

Huntington, J. L., Szilagyi, J., Tyler, S. W., & Pohll, G. M. (2011). Evaluating the complementary relationship for estimating evapotranspiration from arid shrublands. *Water Resources Research*, *47*(5), 1–11. https://doi.org/10.1029/2010WR009874

Iizumi, T., & Ramankutty, N. (2015). How do weather and climate influence cropping area and intensity? *Global Food Security*, *4*, 46–50.

Irmak, S., Hay, D. R., Anderson, B. E., Kranz, W. L., & Dean Yonts, C. (2007). Irrigation management and crop characteristics of alfalfa. *NebGuide G1778. University of Nebraska Lincoln*.

Kam, J., Sheffield, J., & Wood, E. F. (2014). A multiscale analysis of drought and pluvial mechanisms for the southeastern United States. *Journal of Geophysical Research: Atmospheres*, *119*(12), 7348–7367.

Kaufman, J. (2016). *Northeast Farmers Grapple With Worst Drought In More Than A Decade*. NPR. https://www.npr.org/sections/thesalt/2016/08/30/491942025/northeast-farmers-grapple-with-worst-drought-in-more-than-a-decade

Kendall, M. G. (1961). *The advanced theory of statistics: Inference and relationship. Vol. 2* (Vol. 2). C. Griffin.

Kiem, A. S., Johnson, F., Westra, S., van Dijk, A., Evans, J. P., O'Donnell, A., Rouillard, A., Barr, C., Tyler, J., Thyer, M., Jakob, D., Woldemeskel, F., Sivakumar, B., & Mehrotra, R. (2016). Natural hazards in Australia: droughts. *Climatic Change*, *139*(1), 37–54. https://doi.org/10.1007/s10584-016-1798-7

Koster, R. D., & Suarez, M. J. (2001). Soil moisture memory in climate models. *Journal*

of Hydrometeorology, *2*(6), 558–570.

Lacey, K. (2019). *Calculating Readily Available Water*. Agriculture and Food - Government of Western Australia. https://www.agric.wa.gov.au/citrus/calculating-readily-available-water?page=0%2C1

Lickley, M., & Solomon, S. (2018). Drivers, timing and some impacts of global aridity change. *Environmental Research Letters*, *13*(10). https://doi.org/10.1088/1748-9326/aae013

Lin, W. U. (1985). Matching irrigation to turfgrass root depth. *Califomia Turfgrass Culture*, *35*, 1–2.

Lobell, D. B., & Asner, G. P. (2003). Climate and management contributions to recent trends in U. S. agricultural yields. *Science*, *299*(5609), 1032.

Lombard, P. J., Barclay, J. R., & McCarthy, D.-A. E. (2020). 2020 drought in New England. In *Open-File Report* (Version 1.). https://doi.org/10.3133/ofr20201148

Lorenzo-Lacruz, J., Vicente-Serrano, S. M., López-Moreno, J. I., Beguería, S., García-Ruiz, J. M., & Cuadrat, J. M. (2010). The impact of droughts and water management on various hydrological systems in the headwaters of the Tagus River (central Spain). *Journal of Hydrology*, *386*(1–4), 13–26.

Lotter, D. W., Seidel, R., & Liebhardt, W. (2003). The performance of organic and conventional cropping systems in an extreme climate year. *American Journal of Alternative Agriculture*, *18*(3), 146–154. https://doi.org/10.1079/AJAA200345

Lu, J., Carbone, G. J., Huang, X., Lackstrom, K., & Gao, P. (2020). Mapping the sensitivity of agriculture to drought and estimating the effect of irrigation in the United States, 1950–2016. *Agricultural and Forest Meteorology*, *292–293*(May),

108124. https://doi.org/10.1016/j.agrformet.2020.108124

McCabe, G. J., Betancourt, J. L., Gray, S. T., Palecki, M. A., & Hidalgo, H. G. (2008). Associations of multi-decadal sea-surface temperature variability with US drought. *Quaternary International*, *188*(1), 31–40.

McEvoy, D. J., Huntington, J. L., Hobbins, M. T., Wood, A., Morton, C., Anderson, M., & Hain, C. (2016). The Evaporative Demand Drought Index. Part II: CONUS-Wide Assessment against Common Drought Indicators. *Journal of Hydrometeorology*, *17*(6), 1763–1779. https://doi.org/10.1175/JHM-D-15-0122.1

McKee, T. B. (1995). Drought monitoring with multiple time scales. *Proceedings of 9th Conference on Applied Climatology, Boston, 1995*.

McKee, T. B., Doesken, N. J., & Kleist, J. (1993). The relationship of drought frequency and duration to time scales. *Proceedings of the 8th Conference on Applied Climatology*, *17*(22), 179–183.

Millar, C. I., & Stephenson, N. L. (2015). Temperate forest health in an era of emerging megadisturbance. *Science*, *349*(6250), 823–826.

Mishra, A. K., & Singh, V. P. (2010). A review of drought concepts. *Journal of Hydrology*, *391*(1–2), 202–216.

Moden, C. (2017). *Officials Announce Drought is Over in New York*. WYRK. https://wyrk.com/officials-announce-drought-is-over-in-new-york/

Monteith, J. L. (1965). Evaporation and environment. *Symposia of the Society for Experimental Biology*, *19*, 205–234.

Mounce, R. B., O'Shaughnessy, S. A., Blaser, B. C., Colaizzi, P. D., & Evett, S. R. (2016). Crop response of drought-tolerant and conventional maize hybrids in a

semiarid environment. *Irrigation Science*, *34*(3), 231–244.

Namias, J. (1966). Nature and possible causes of the northeastern United States drought during 1962–65. *Monthly Weather Review*, *94*(9), 543–554.

Narasimhan, B., & Srinivasan, R. (2005). Development and evaluation of Soil Moisture Deficit Index (SMDI) and Evapotranspiration Deficit Index (ETDI) for agricultural drought monitoring. *Agricultural and Forest Meteorology*, *133*(1–4), 69–88.

Naresh Kumar, M., Murthy, C. S., Sesha Sai, M. V. R., & Roy, P. S. (2009). On the use of Standardized Precipitation Index (SPI) for drought intensity assessment. *Meteorological Applications: A Journal of Forecasting, Practical Applications, Training Techniques and Modelling*, *16*(3), 381–389.

NASS, U. (2016a). *Quick stats*. USDA-NASS, Washington, DC. https://quickstats.nass.usda.gov/

NASS, U. (2016b). USDA national agricultural statistics service cropland data layer. *Publ. Crop. Data Layer. URL Https://Nassgeodata. Gmu. Edu/CropScape/(Accessed 5.18. 16)*.

NCDC. (2022). *NOAA National Centers for Environmental information, Climate at a Glance: Statewide Time Series*. https://www.ncdc.noaa.gov/cag/

NDMC. (2021). *National Drought Mitigation Center*. https://drought.unl.edu/Home.aspx

NIDIS. (2020). *DEWS Regions Drought Information*. https://www.drought.gov/dews

NIDIS, & NOAA. (2019). *NORTHEAST DROUGHT EARLY WARNING SYSTEM 2018-2019 Strategic Plan*. https://www.drought.gov/documents/2018-2019-northeast-dews-strategic-plan

Nielsen-Gammon, J. W. (2012). The 2011 texas drought. *Texas Water Journal*, *3*(1), 59–

95.

Nosowitz, D. (2016). *Insanely Bad Summer Drought is Decimating New England Farms*. Modern Farmer. https://modernfarmer.com/2016/10/new-england-drought/

NRCC. (2011). *Climate Perspectives and Evapotranspiration Averages*. https://www.nrcc.cornell.edu/wxstation/pet/pet.html

NRCC. (2017). *Northeast drought assesment: 2016-2017*. https://www.nrcc.cornell.edu/regional/drought/pubs/assessment_2016.pdf

NRCC. (2021). *State & Regional Analysis*. https://www.nrcc.cornell.edu/

Orr, S. (2016). *This summer was one to remember*. Democrat & Chronicle. https://www.democratandchronicle.com/story/news/2016/08/31/this-summer-was-one-to-remember/89408616/

Park Williams, A., Cook, B. I., Smerdon, J. E., Bishop, D. A., Seager, R., & Mankin, J. S. (2017). The 2016 southeastern US drought: An extreme departure from centennial wetting and cooling. *Journal of Geophysical Research: Atmospheres*, *122*(20), 10–888.

Pasho, E., Camarero, J. J., de Luis, M., & Vicente-Serrano, S. M. (2011). Impacts of drought at different time scales on forest growth across a wide climatic gradient in north-eastern Spain. *Agricultural and Forest Meteorology*, *151*(12), 1800–1811.

Peña-Gallardo, M., Vicente-Serrano, S. M., Domínguez-Castro, F., Quiring, S., Svoboda, M., Beguería, S., & Hannaford, J. (2018). Effectiveness of drought indices in identifying impacts on major crops across the USA. *Climate Research*, *75*(3), 221–240.

Peña-Gallardo, M., Vicente-Serrano, S. M., Quiring, S., Svoboda, M., Hannaford, J.,

Tomas-Burguera, M., Martín-Hernández, N., Domínguez-Castro, F., & El Kenawy, A. (2019). Response of crop yield to different time-scales of drought in the United States: Spatio-temporal patterns and climatic and environmental drivers. *Agricultural and Forest Meteorology*, *264*(September 2018), 40–55. https://doi.org/10.1016/j.agrformet.2018.09.019

Pendergrass, A. G., Meehl, G. A., Pulwarty, R., Hobbins, M., Hoell, A., AghaKouchak, A., Bonfils, C. J. W., Gallant, A. J. E., Hoerling, M., Hoffmann, D., Kaatz, L., Lehner, F., Llewellyn, D., Mote, P., Neale, R. B., Overpeck, J. T., Sheffield, A., Stahl, K., Svoboda, M., … Woodhouse, C. A. (2020). Flash droughts present a new challenge for subseasonal-to-seasonal prediction. *Nature Climate Change*, *10*(3), 191–199. https://doi.org/10.1038/s41558-020-0709-0

Potopová, V., Boroneanţ, C., Boincean, B., & Soukup, J. (2016). Impact of agricultural drought on main crop yields in the Republic of Moldova. *International Journal of Climatology*, *36*(4), 2063–2082. https://doi.org/10.1002/joc.4481

Praskievicz, S., & Sigdel, R. (2021). Loading of stream wood following the 2016 Chimney Tops 2 Wildfire: Great Smoky Mountains National Park, Tennessee, USA. *River Research and Applications*, *37*(3), 475–483.

Qin, Y., Abatzoglou, J. T., Siebert, S., Huning, L. S., AghaKouchak, A., Mankin, J. S., Hong, C., Tong, D., Davis, S. J., & Mueller, N. D. (2020). Agricultural risks from changing snowmelt. *Nature Climate Change*, *10*(5), 459–465.

Ramadas, M., & Govindaraju, R. S. (2015). Probabilistic assessment of agricultural droughts using graphical models. *Journal of Hydrology*, *526*, 151–163.

Rangwala, I., Smith, L. L., Senay, G., Barsugli, J., Kagone, S., & Hobbins, M. (2019).

Landscape Evaporative Response Index (LERI): A high resolution monitoring and assessment of evapotranspiration across the Contiguous United States. *U.S. Geological Survey ScienceBase*. https://doi.org/https://doi.org/10.21429/43r4-3q68

Robock, A., Luo, L., Wood, E. F., Wen, F., Mitchell, K. E., Houser, P. R., Schaake, J. C., Lohmann, D., Cosgrove, B., & Sheffield, J. (2003). Evaluation of the North American Land Data Assimilation System over the southern Great Plains during the warm season. *Journal of Geophysical Research: Atmospheres*, *108*(D22).

Robock, A., Vinnikov, K. Y., Srinivasan, G., Entin, J. K., Hollinger, S. E., Speranskaya, N. A., Liu, S., & Namkhai, A. (2000). The global soil moisture data bank. *Bulletin of the American Meteorological Society*, *81*(6), 1281–1300.

Rosales, A. (2021). *Crop Progress and Condition Layers*. https://www.nass.usda.gov/Research_and_Science/Crop_Progress_Gridded_Layers/CropProgressDescription.pdf

Rotstayn, L. D., Roderick, M. L., & Farquhar, G. D. (2006). A simple pan-evaporation model for analysis of climate simulations: Evaluation over Australia. *Geophysical Research Letters*, *33*(17).

Sánchez, N., González-Zamora, Á., Piles, M., & Martínez-Fernández, J. (2016). A new Soil Moisture Agricultural Drought Index (SMADI) integrating MODIS and SMOS products: a case of study over the Iberian Peninsula. *Remote Sensing*, *8*(4), 287.

Schaake, J. C., Duan, Q., Koren, V., Mitchell, K. E., Houser, P. R., Wood, E. F., Robock, A., Lettenmaier, D. P., Lohmann, D., & Cosgrove, B. (2004). An intercomparison of soil moisture fields in the North American Land Data Assimilation System (NLDAS). *Journal of Geophysical Research: Atmospheres*, *109*(D1).

Seager, R. (2007). The turn of the century North American drought: Global context, dynamics, and past analogs. *Journal of Climate*, *20*(22), 5527–5552. https://doi.org/10.1175/2007JCLI1529.1

Seager, R., Hoerling, M., Schubert, S., Wang, H., Lyon, B., Kumar, A., Nakamura, J., & Henderson, N. (2015). Causes of the 2011–14 California drought. *Journal of Climate*, *28*(18), 6997–7024.

Seager, R., Naik, N., & Vogel, L. (2012). Does global warming cause intensified interannual hydroclimate variability? *Journal of Climate*, *25*(9), 3355–3372. https://doi.org/10.1175/JCLI-D-11-00363.1

Seager, R., Pederson, N., Kushnir, Y., Nakamura, J., & Jurburg, S. (2012). The 1960s drought and the subsequent shift to a wetter climate in the Catskill Mountains region of the New York City watershed. *Journal of Climate*, *25*(19), 6721–6742. https://doi.org/10.1175/JCLI-D-11-00518.1

Senay, G. B., Bohms, S., Singh, R. K., Gowda, P. H., Velpuri, N. M., Alemu, H., & Verdin, J. P. (2013). Operational Evapotranspiration Mapping Using Remote Sensing and Weather Datasets: A New Parameterization for the SSEB Approach. *Journal of the American Water Resources Association*, *49*(3), 577–591. https://doi.org/10.1111/jawr.12057

Sepulcre-Canto, G., Horion, S., Singleton, A., Carrao, H., & Vogt, J. (2012). Development of a Combined Drought Indicator to detect agricultural drought in Europe. *Natural Hazards and Earth System Sciences*, *12*(11), 3519–3531.

Sharma, T. C., & Panu, U. S. (2012). Prediction of hydrological drought durations based on Markov chains: case of the Canadian prairies. *Hydrological Sciences Journal*,

57(4), 705–722.

Sheffield, J., Goteti, G., Wen, F., & Wood, E. F. (2004). A simulated soil moisture based drought analysis for the United States. *Journal of Geophysical Research: Atmospheres*, *109*(D24).

Sheffield, J., & Wood, E. F. (2008). Global trends and variability in soil moisture and drought characteristics, 1950–2000, from observation-driven simulations of the terrestrial hydrologic cycle. *Journal of Climate*, *21*(3), 432–458.

Silverman, B. W. (2018). *Density estimation for statistics and data analysis*. Routledge.

Simelton, E., Fraser, E. D. G., Termansen, M., Forster, P. M., & Dougill, A. J. (2009). Typologies of crop-drought vulnerability: an empirical analysis of the socio-economic factors that influence the sensitivity and resilience to drought of three major food crops in China (1961–2001). *Environmental Science & Policy*, *12*(4), 438–452.

Skamarock, W. C., Klemp, J. B., Dudhia, J., Gill, D. O., Liu, Z., Berner, J., Wang, W., Powers, J. G., Duda, M. G., & Barker, D. M. (2019). A description of the advanced research WRF model version 4. *National Center for Atmospheric Research: Boulder, CO, USA*, *145*, 145.

Sousa, P. M., Blamey, R. C., Reason, C. J. C., Ramos, A. M., & Trigo, R. M. (2018). The 'Day Zero'Cape Town drought and the poleward migration of moisture corridors. *Environmental Research Letters*, *13*(12), 124025.

Stewart, I. T. (2009). Changes in snowpack and snowmelt runoff for key mountain regions. *Hydrological Processes: An International Journal*, *23*(1), 78–94.

Sun, Y., Fu, R., Dickinson, R., Joiner, J., Frankenberg, C., Gu, L., Xia, Y., & Fernando,

N. (2015). Drought onset mechanisms revealed by satellite solar-induced chlorophyll fluorescence: Insights from two contrasting extreme events. *Journal of Geophysical Research: Biogeosciences*, *120*(11), 2427–2440. https://doi.org/10.1002/2015JG003150

Svoboda, M., LeComte, D., Hayes, M., Heim, R., Gleason, K., Angel, J., Rippey, B., Tinker, R., Palecki, M., Stooksbury, D., Miskus, D., & Stephens, S. (2002). THE DROUGHT MONITOR. *Bulletin of the American Meteorological Society*, *83*(8), 1181–1190. https://doi.org/10.1175/1520-0477-83.8.1181

Sweet, S. K., Wolfe, D. W., DeGaetano, A., & Benner, R. (2017). Anatomy of the 2016 drought in the Northeastern United States: Implications for agriculture and water resources in humid climates. *Agricultural and Forest Meteorology*, *247*(August), 571–581. https://doi.org/10.1016/j.agrformet.2017.08.024

Sweet, S., & Wolfe, D. (2017). *Anatomy of a Rare Drought: Insights from New York Farmers. CICSS Research and Policy Brief: Issue 3*.

Trenberth, K. E., Dai, A., Van Der Schrier, G., Jones, P. D., Barichivich, J., Briffa, K. R., & Sheffield, J. (2014). Global warming and changes in drought. *Nature Climate Change*, *4*(1), 17–22.

Trnka, M., Hlavinka, P., Možný, M., Semerádová, D., Štěpánek, P., Balek, J., Bartošová, L., Zahradníček, P., Bláhová, M., & Skalák, P. (2020). Czech Drought Monitor System for monitoring and forecasting agricultural drought and drought impacts. *International Journal of Climatology*, *40*(14), 5941–5958.

USDA. (2013). Drought 2012 : Farm and Food Impacts. In *USDA Economic Research Service*. https://drought.unl.edu/archive/assessments/USDA-ERS-2012-farm-food-

impacts.pdf

USDA. (2018). *National Agricultural Statistic Service*. https://www.nass.usda.gov/index.php

USDA. (2019). *2017 Census of Agriculture: 2018 irrigation and water management survey*. https://www.nass.usda.gov/Publications/AgCensus/2017/Online_Resources/Farm_and_Ranch_Irrigation_Survey/fris.pdf

USDA. (2021). *Northeast Climate Hub*. https://www.climatehubs.usda.gov/hubs/northeast/drought-map

USGS. (2021). *WaterWatch*. https://waterwatch.usgs.gov/index.php

Van Loon, A. F. (2015). Hydrological drought explained. *Wiley Interdisciplinary Reviews: Water, 2*(4), 359–392.

Van Loon, A. F., & Van Lanen, H. A. J. (2012). A process-based typology of hydrological drought. *Hydrology and Earth System Sciences, 16*(7), 1915–1946.

Vicente-Serrano, S. M., Beguería, S., & López-Moreno, J. I. (2010). A multiscalar drought index sensitive to global warming: The standardized precipitation evapotranspiration index. *Journal of Climate, 23*(7), 1696–1718. https://doi.org/10.1175/2009JCLI2909.1

Vicente-Serrano, S. M., Beguería, S., Lorenzo-Lacruz, J., Camarero, J. J., López-Moreno, J. I., Azorin-Molina, C., Revuelto, J., Morán-Tejeda, E., & Sanchez-Lorenzo, A. (2012). Performance of drought indices for ecological, agricultural, and hydrological applications. *Earth Interactions, 16*(10), 1–27.

Vicente-Serrano, S. M., Gouveia, C., Camarero, J. J., Beguería, S., Trigo, R., López-

Moreno, J. I., Azorín-Molina, C., Pasho, E., Lorenzo-Lacruz, J., & Revuelto, J. (2013). Response of vegetation to drought time-scales across global land biomes. *Proceedings of the National Academy of Sciences*, *110*(1), 52–57.

Walter, I. A., Allen, R. G., Elliott, R., Itenfisu, D., Brown, P., Jensen, M. E., Mecham, B., Howell, T. A., Snyder, R., & Eching, S. (2005). Task committee on standardization of reference evapotranspiration. *ASCE: Reston, VA, USA*.

Walter, I. A., Allen, R. G., Elliott, R., Jensen, M. E., Itenfisu, D., Mecham, B., Howell, T. A., Snyder, R., Brown, P., Echings, S., Spofford, T., Hattendorf, M., Cuenca, R. H., Wright, J. L., & Martin, D. (2001). ASCE's Standardized Reference Evapotranspiration Equation. *Watershed Management and Operations Management 2000*, *105*(May), 1–11. https://doi.org/10.1061/40499(2000)126

Wang, Q., Wu, J., Lei, T., He, B., Wu, Z., Liu, M., Mo, X., Geng, G., Li, X., & Zhou, H. (2014). Temporal-spatial characteristics of severe drought events and their impact on agriculture on a global scale. *Quaternary International*, *349*, 10–21.

Wetterhall, F., Winsemius, H. C., Dutra, E., Werner, M., & Pappenberger, E. (2015). Seasonal predictions of agro-meteorological drought indicators for the Limpopo basin. *Hydrology and Earth System Sciences*, *19*(6), 2577–2586.

Wilhite, D. A. (2000). *Drought. A global assessment for drought*. Westview Press, Boulder.

Wilhite, D. A., & Glantz, M. H. (1985). Understanding: the drought phenomenon: the role of definitions. *Water International*, *10*(3), 111–120.

Wilks, D. S. (2011). Empirical distributions and exploratory data analysis. In *International Geophysics* (Vol. 100, pp. 23–70). Elsevier.

Williams, A. P., Seager, R., Macalady, A. K., Berkelhammer, M., Crimmins, M. A., Swetnam, T. W., Trugman, A. T., Buenning, N., Noone, D., & McDowell, N. G. (2014). Correlations between components of the water balance and burned area reveal new insights for predicting forest fire area in the southwest United States. *International Journal of Wildland Fire*, *24*(1), 14–26.

Wu, H., Hayes, M. J., Wilhite, D. A., & Svoboda, M. D. (2005). The effect of the length of record on the standardized precipitation index calculation. *International Journal of Climatology: A Journal of the Royal Meteorological Society*, *25*(4), 505–520.

Wu, H., Hubbard, K. G., & Wilhite, D. A. (2004). An agricultural drought risk-assessment model for corn and soybeans. *International Journal of Climatology*, *24*(6), 723–741. https://doi.org/10.1002/joc.1028

Wu, W., & Dickinson, R. E. (2004). Time scales of layered soil moisture memory in the context ofland–atmosphere interaction. *Journal of Climate*, *17*(14), 2752–2764.

Wurster, P., Maneta, M., Beguería, S., Cobourn, K., Maxwell, B., Silverman, N., Ewing, S., Jensco, K., Gardner, P., Kimball, J., Holden, Z., Ji, X., & Vicente-Serrano, S. M. (2020). Characterizing the impact of climatic and price anomalies on agrosystems in the northwest United States. *Agricultural and Forest Meteorology*, *280*(September 2019), 107778. https://doi.org/10.1016/j.agrformet.2019.107778

Xia, Y., Mitchell, K., Ek, M., Cosgrove, B., Sheffield, J., Luo, L., Alonge, C., Wei, H., Meng, J., Livneh, B., Duan, Q., & Lohmann, D. (2012). Continental-scale water and energy flux analysis and validation for North American Land Data Assimilation System project phase 2 (NLDAS-2): 2. Validation of model-simulated streamflow. *Journal of Geophysical Research: Atmospheres*, *117*(D3), n/a-n/a.

https://doi.org/10.1029/2011JD016051

Xia, Y., Sheffield, J., Ek, M. B., Dong, J., Chaney, N., Wei, H., Meng, J., & Wood, E. F. (2014). Evaluation of multi-model simulated soil moisture in NLDAS-2. *Journal of Hydrology*, *512*, 107–125. https://doi.org/10.1016/j.jhydrol.2014.02.027

Yamoah, C. F., Walters, D. T., Shapiro, C. A., Francis, C. A., & Hayes, M. J. (2000). Standardized precipitation index and nitrogen rate effects on crop yields and risk distribution in maize. *Agriculture, Ecosystems & Environment*, *80*(1–2), 113–120.

Yang, J., & Zhang, J. (2006). Grain filling of cereals under soil drying. *New Phytologist*, *169*(2), 223–236.

Yuan, X., Wang, L., Wu, P., Ji, P., Sheffield, J., & Zhang, M. (2019). Anthropogenic shift towards higher risk of flash drought over China. *Nature Communications*, *10*(1), 1–8.

Zhao, A., Zhang, A., Cao, S., Liu, X., Liu, J., & Cheng, D. (2018). Responses of vegetation productivity to multi-scale drought in Loess Plateau, China. *Catena*, *163*, 165–171.

Zipper, S. C., Qiu, J., & Kucharik, C. J. (2016). Drought effects on US maize and soybean production: spatiotemporal patterns and historical changes. *Environmental Research Letters*, *11*(9), 94021.